Biomaterials 131 (2017) 160–175

Contents lists available at ScienceDirect

Biomaterials

journal homepage: www.elsevier.com/locate/biomaterials

Local induction of lymphangiogenesis with engineered fibrin-binding VEGF-C promotes wound healing by increasing immune cell trafficking and matrix remodeling

Esra Güç [a, b], Priscilla S. Briquez [a], Didier Foretay [a], Manuel A. Fankhauser [a], Jeffrey A. Hubbell [a, c], Witold W. Kilarski [c, *, 1], Melody A. Swartz [a, c, d, **, 1]

[a] Institute of Bioengineering and Swiss Institute for Experimental Cancer Research (ISREC), École Polytechnique Fédérale de Lausanne (EPFL), Lausanne, Switzerland
[b] MRC Centre for Reproductive Health, Queen's Medical Research Institute, The University of Edinburgh, Edinburgh, UK
[c] Institute for Molecular Engineering, The University of Chicago, Chicago, IL, USA
[d] Ben May Department of Cancer Research, The University of Chicago, Chicago, IL, USA

ARTICLE INFO

Article history:
Received 12 January 2017
Received in revised form
21 March 2017
Accepted 21 March 2017
Available online 25 March 2017

Keywords:
VEGF-C
Fibrin
Lymphatics
Regenerative medicine

ABSTRACT

Lymphangiogenesis occurs in inflammation and wound healing, yet its functional roles in these processes are not fully understood. Consequently, clinically relevant strategies for therapeutic lymphangiogenesis remain underdeveloped, particularly using growth factors. To achieve controlled, local capillary lymphangiogenesis with protein engineering and determine its effects on fluid clearance, leukocyte trafficking, and wound healing, we developed a fibrin-binding variant of vascular endothelial growth factor C (FB-VEGF-C) that is slowly released upon demand from infiltrating cells. Using a novel wound healing model, we show that implanted fibrin containing FB-VEGF-C, but not free VEGF-C, could stimulate local lymphangiogenesis in a dose-dependent manner. Importantly, the effects of FB-VEGF-C were restricted to lymphatic capillaries, with no apparent changes to blood vessels and downstream collecting vessels. Leukocyte intravasation and trafficking to lymph nodes were increased in hyperplastic lymphatics, while fluid clearance was maintained at physiological levels. In diabetic wounds, FB-VEGF-C-induced lymphangiogenesis increased extracellular matrix deposition and granulation tissue thickening, indicators of improved wound healing. Together, these results indicate that FB-VEGF-C is a promising strategy for inducing lymphangiogenesis locally, and that such lymphangiogenesis can promote wound healing by enhancing leukocyte trafficking without affecting downstream lymphatic collecting vessels.

1. Introduction

Lymphatic vessels provide transport routes for immune cells, macromolecules and fluid from the periphery of the body to the lymph nodes and eventually back to the blood. In addition, lymphatic endothelial cells (LECs) can modulate immune cell trafficking and function by secreting chemokines, regulating surface and junctional adhesion molecules for leukocyte transmigration, expressing stimulatory and inhibitory receptors, and presenting antigens to T cells [1,2]. Lymphatic vessel expansion, also called lymphangiogenesis, is driven by multiple factors, including VEGF-C and VEGF-D, which are ligands of vascular endothelial growth factor receptor 3 (VEGFR-3) [3,4]. Lymphangiogenesis occurs post-developmentally in wound healing, chronic inflammation, and cancer [5].

In dermal wound healing, a tissue-deposited fibrin clot is initially infiltrated by innate immune cells (*i.e.*, neutrophils, monocytes, and macrophages) to be populated by anti-inflammatory macrophages and myofibroblasts. These healing-specific contractile cells cleave fibrin and remodel the new matrix in wounds, and their population declines when the mechanical tension is removed [6]. The appearance of myofibroblasts is followed by an

* Corresponding author. Institute of Molecular Engineering, 5640 S. Ellis Ave., Chicago, IL 60637, USA.
** Corresponding author. Institute of Molecular Engineering, 5640 S. Ellis Ave., Chicago, IL 60637, USA.
E-mail addresses: wkilarski@uchicago.edu (W.W. Kilarski), melodyswartz@uchicago.edu (M.A. Swartz).
[1] Authors equally contributed to this work.

http://dx.doi.org/10.1016/j.biomaterials.2017.03.033

Non-standard abbreviations and acronyms

FB-VEGF-C	Fibrin-binding variant of vascular endothelial growth factor C
LECs	Lymphatic endothelial cells
VEGFR-3	Vascular endothelial growth factor receptor 3
MMP	Matrix metalloproteinase
FXIIIa	Factor XIIIa
α_2-PI	α_2-plasmin inhibitor
GT	Granulation tissue
DC	Dendritic cells
BECs	Blood endothelial cells

ingrowth of transient blood vessels to meet increasing demands for oxygen and nutrients for the support and surveillance of tissue repair. Mechanisms of rapid restoration of blood circulation in wound healing include tension-dependent looping angiogenesis with sprouting and intussusception [7,8]. In contrast, lymphatic vessel regeneration is less well studied [9,10]. Therefore, even though it is well established that lymphangiogenesis follows angiogenesis in wound healing [11–13], the precise roles for the restored lymphatic vasculature in wound healing remain unclear.

We previously showed that increased interstitial fluid flow, such as that generated in inflamed or healing tissues, can stimulate myofibroblasts differentiation and matrix alignment [14]. In turn, this could increase directional wound contractility and vascularization, possibly through a force-dependent vessel looping mechanism that accelerates the healing process [6,15]. We assume that wound-associated lymphangiogenesis could alter immune cell trafficking from the wound, since lymphatic expression of adhesion molecules like E-selectin and ICAM-1 regulate leukocyte emigration [16], along with Lyve-1, a hyaluronan receptor expressed predominantly on initial lymphatics [17]. In turn, changes in leukocyte trafficking could affect the local profiles of cell-derived signals and the production of cytokines and growth factors that directly stimulate matrix remodeling.

Previously, it was shown that reduced lymphatic vessel formation contributes to impaired diabetic skin wound healing [18]. However, few studies have explored therapeutic lymphangiogenesis as a potential means to improve healing in such diabetic wounds, which are resistant to healing and develop high interstitial fluid pressure [19,20]. In models where lymphatic vessels were ablated, local delivery of recombinant VEGF-C was shown to improve healing and reduce tissue edema [21], and adenovirally delivered VEGF-C expedited reconnection of lymphatic vessels after lymph node dissection [19]. Interestingly, adenoviral overexpression of VEGF-C in skin diabetic wounds was shown to stimulate their healing, predominantly by the activation of blood vessel angiogenesis and local attraction of macrophages [20]. These results established the therapeutic potential of VEGF-C.

The local delivery of lymphangiogenic growth factors remains a challenge in clinical translation. To date, most studies with *in vivo* delivery of VEGF-C to induce lymphangiogenesis have used adenoviral vectors [10]. However, with viral vectors it is difficult to control dose, and the risk of unpredictable immune responses against the virus-based vehicles is an obstacle for patient translation [22]. For protein delivery, wild-type proteins rapidly diffuse from the injection site and cannot be maintained locally for more than a day [23], and repeated high-dose administration of VEGF-C could lead to edema and venous enlargement because higher doses of VEGF-C can induce pathological permeability and hyperplasia of blood vessels [24,25] as well as dysfunctional remodeling of collecting lymphatic vessels [19,26].

Over the last two decades, new approaches used in growth factor engineering for wound healing have been developed [23,27]. In particular, the immobilization of a growth factor to a biopolymer or to extracellular matrix components enables its local and cell-demanded release by augmenting its binding to cell surface receptors and creating local gradients that mimic those of endogenously released growth factors within the extracellular environment [28]. One well-established method is the recombinant fusion of a substrate sequence for the coagulation transglutaminase Factor XIIIa (FXIIIa), the substrate being derived from α_2-plasmin inhibitor (α_2-PI, where the substrate is α_2-$PI_{1\text{-}8}$), to exogenous growth factors. These growth factors can then be covalently attached to fibrin through FXIIIa during polymerization and are released only when fibrin is proteolytically cleaved during remodeling [29]. This approach diminishes the need for the application of high doses of growth factors and prevents growth factor toxicity. Furthermore, the fibrin matrix supports cell migration and proliferation and is completely cleared when healing is completed [30]. Nevertheless, no strategy that immobilizes VEGF-C within the fibrin matrix has been implemented for lymphangiogenic therapy.

Here, we developed a fibrin-binding VEGF-C variant, in which the FXIIIa substrate sequence α_2-$PI_{1\text{-}8}$ and a matrix metalloproteinase (MMP)-degradable domain are inserted, and explore its therapeutic applications. With this design, VEGF-C can be released by either the plasmin-mediated cleavage of fibrin or MMP-mediated cleavage of the substrate peptide fused between α_2-$PI_{1\text{-}8}$ and VEGF-C, referred to as FB-VEGF-C. We found that new functional initial lymphatic vessels could be specifically induced with a low-dose, single implantation of FB-VEGF-C in a subcutaneous cartilage-replacement healing model. The pro-lymphangiogenic effects were local and only affected lymphatic capillaries, not downstream collecting vessels, which further provided the opportunity to conduct a comprehensive study of the morphology and function of the newly formed lymphatic capillaries. To do that, we developed a functional assay that tests the ability of newly formed initial vessels to attract dendritic cells (DC) and further evacuate them from the healed wound to the draining lymph node. We also established an imaging method for the morphological analysis of the entire draining collecting vessel system, from the initial lymphatic bed down to the draining lymph node. Finally, we designed an assay that aimed to quantify lymphatic fluid drainage at the physiological interstitial fluid pressure, or without an injection swelling pressure, which would reveal dysfunctions in the lymphatic vasculature. Similarly to the newly formed lymphatics in control wounds, hyperplastic lymphatics in FB-VEGF-C-healed wounds attracted DCs that could transmigrate to the lymphatic lumen. The net migration towards the draining lymph node was increased via FB-VEGF-C-healed lymphatics, while the lymphatic clearance remained unchanged. Importantly, in diabetic mice, the local delivery of FB-VEGF-C in impaired wounds improved granulation tissue (GT) formation and increased the interaction of immune cells with activated lymphatic vessels. Together, these findings suggest that FB-VEGF-C is effective at inducing lymphangiogenesis locally, only within initial lymphatics, and such engineered local lymphangiogenesis holds therapeutic promise for impaired wound healing.

2. Methods

2.1. Mice

All experiments were carried out according to a protocol approved by the Committee for Animal Experiments for the Canton

Vaud, Switzerland. 8-12-week-old female Balb/c mice (Charles River, Orleans, France) were used for all studies except for the full thickness diabetic wound healing studies, where C57BLKS/J-m/Lepr db (*db/db*) mice were used.

2.2. Cell culture

Human dermal LECs were isolated from neonatal foreskin using anti-CD31 and anti-podoplanin antibodies (Invitrogen, Carlsbad, CA), and authenticated as described earlier [31]. Cells were expanded on collagen-coated flasks in basal endothelial cell medium (Lonza, Verviers, Belgium) supplemented with 20% fetal bovine serum (FBS, Gibco Invitrogen, Grand Island, NY) and 1 mg/ml hydrocortisone acetate (Sigma-Aldrich, St. Louis, MO), 25 mg/ml dibutyril cAMP (Sigma-Aldrich), and 1% penicillin, streptomycin, amphotericin (Invitrogen). Cells were grown at 37 °C in a 5% CO_2 incubator and were used at passage 6–9. Cells tested negative for mycoplasma contamination.

2.3. Cloning of VEGF-C variants

The transglutaminase substrate domain from α_2-plasmin inhibitor $\alpha_2PI_{1\text{-}8}$; NQEQVSPL [32], and the MMP degradable domain derived from peptide library (GPQGIWGQ) [33] were fused to the N-terminus of VEGF-C. FB*-VEGF-C ($\alpha_2PI_{1\text{-}8}$-VEGF-C), FB-VEGF-C ($\alpha_2PI_{1\text{-}8}$-MMP-VEGF-C) and VEGF-C were expressed in HEK293 cells by insertion of the pXLG vector expressing cDNA with the addition of an N-terminus 8× His-tag. Protein was purified using a HisTrap HP™ column (GE Healthcare, Glattbrugg, Switzerland). Low endotoxin levels (EU < 0.1 per dose administration) were confirmed by endotoxin in HEK-Blue hTLR 4 cells from InvivoGen (San Diego, CA). The concentration of the protein was determined using a Nanodrop spectrophotometer (Thermo Scientific, Waltham, MA) and protein molecular weight. The purity was verified by SDS-PAGE and SimplyBlue SafeStain (Invitrogen).

2.4. VEGFR-3 phosphorylation assay

LECs were seeded in 6-well plates (7.5×10^4 cells per well) and starved in medium containing 1% serum overnight followed by serum-free medium containing 0.5% bovine serum albumin (BSA) (Sigma-Aldrich) for 4 h before the stimulation. 100 ng/ml of each of the VEGF-C variants (VEGF-C, FB*-VEGF-C or FB-VEGF-C) was applied to the cells for 5, 10 and 15 min. Cells were washed with ice-cold phosphate buffered saline (PBS) and immediately lysed in 1% NP-40, 20 mM Tris (pH 8.0), and 137 mM NaCl. A solution of 10% Glycerol, 2 mM EDTA, 1 mM activated sodium orthovanadate and EDTA free protease cocktail inhibitors (Roche Diagnostics, Mannheim, Germany) at 4 °C was then added and kept on ice for 15 min. Samples were stored at −80 °C before VEGFR-3 phosphorylation was measured using Human Phospho-VEGFR3/Flt-4 ELISA kits (R&D Systems, Minneapolis, MN).

2.5. Cell proliferation assay

5×10^3 cells were seeded in a 96-well plate and starved with 2% FBS overnight. Cells were then washed with PBS and stimulated with 100 ng/ml of each of the VEGF-C variants in 0.5% BSA for 24 h. AlamarBlue (AbD Serotec, Raleigh, NC) reagent was added to 10% of the total volume and cells were incubated at 37 °C for 4 h before the end of the experiment. The fluorescence change due to metabolic activity was measured with a fluorescence plate reader (Safire II, Tecan, Zurich, Switzerland) according to manufacturers' instructions.

2.6. In vitro 3D lymphangiogenesis in radial flow chamber

The radial flow chamber was prepared as described previously [34]. Fibrin gels were prepared by mixing 3 mg/ml human fibrinogen (Sigma-Aldrich, and fibrinogen solutions were prepared as described previously [35,36]), 2 U/ml human thrombin (Sigma-Aldrich), 2.5 mM $CaCl_2$, 2 U/ml human FXIIIa (CSL Behring, King of Prussia, PS), 100 ng/ml wild-type VEGF-C, FB*-VEGF-C or FB-VEGF-C and 1.5×10^6 cells/ml of human LECs. The mixture was immediately injected into the center of the radial flow chamber and allowed to polymerize. Chambers were kept in static conditions for 18 h to allow for cell attachment and spreading before interstitial flow was initiated. Medium was supplemented with 200 kIU/ml aprotinin (Sigma-Aldrich) and the medium reservoir was changed at every 2 days. 6 days later, cells were fixed with 2% para-formaldehyde for 1 h at room temperature and fixed samples were stained with phalloidin Alexa Fluor® 488 and DAPI (Invitrogen).

2.7. In vivo release kinetics of VEGF-C from fibrin matrix

Wild-type VEGF-C, FB*-VEGF-C and FB-VEGF-C were conjugated by -N-hydroxy-succinimide (NHS) with Alexa Fluor® 680 (Invitrogen). 50 nmol conjugate was used per 1 nmol of protein and samples were incubated at room temperature in the dark for 2 h. Unconjugated dye was then removed using a Zeba Spin desalting column (7 kDa molecular-weight cut-off, Thermo-Fisher, Waltham, MA). Protein concentration was determined using a Nanodrop spectrophotometer (Thermo-Fisher).

For *in vivo* release kinetics, fibrin gels were first prepared in vitro. 40 μg/ml of the VEGF-C variants were mixed with 10 mg/ml fibrinogen, 4 U/ml factor XIIIa, 25 μg/ml aprotinin, 2 U/ml thrombin, and 5 mM $CaCl_2$. 50 μl gel droplets were first prepared and incubated for 15 min at 37 °C before implantation. For implantation, two 0.5 cm diameter cuts were made in the skin. The dermis was detached from the peritoneum with a sterile spatula and a single gel was placed in the pockets. The skin was then sutured and the release of VEGF-C, as measured by the decay in fluorescence over time, was monitored daily using an *in vivo* optical imaging systems (IVIS, Perkin Elmer, Waltham MA, USA). The radiance efficiency units were calculated using Living Image Software 4.0 (Caliper Life Sciences, Waltham, MA).

2.8. Lymphangiogenesis in subcutaneous cartilage-replacement healing model

Hydrogel preparation: Fibrin (5 mg/ml) and rat tail collagen I (2.5 mg/ml) gel mix was prepared using human fibrinogen (Sigma-Aldrich), 2 U/ml FXIIIa (CSL Behring), 2 U/ml thrombin (Sigma-Aldrich), 10 μM aprotinin- $\alpha_2PI_{1\text{-}8}$ [37], 2 mM $CaCl_2$ and rat tail collagen I at 7.5 pH (BD Biosciences, San Jose, CA) and 5 μg/ml wild-type VEGF-C or FB-VEGF-C was used. *Procedure:* Mice were anesthetized using intraperitoneal injection of dormitore (0.05 mg/ml) and ketamine (12.5 mg/ml) in saline solution. The head and ear of the mice were shaved and the excess hair was removed by depilation cream. The ear was placed on a glass platform and the two edges of the ventral side were taped on the glass. The ear dermis was cut in a square shape by making three scalpel incisions, each 0.5 cm long, on the center of ventral side of the ear (center measured between edges of the ear and its antihelix) at the anterior, posterior and distal end of the square wound. The dermis flap was peeled from the cartilage, thus exposing the dorsal dermis to the air. The resulting skin flap was attached to proximal end of the ventral ear and used to cover the implanted gel. The wound and the bleeding was cleaned using Ringer's buffer. 8 μl of hydrogel was applied on the opened window. The solution was allowed to gel for

1–2 min while the ear-flap and air exposed dermis were kept humid. The ear-flap was gently placed back over the gel and three edges were fixed to the remaining ventral skin with surgical glue. 21 days later mice were either used for lymphatic drainage and DC migration assays or euthanized by CO_2, fixed, perfused and ear dermis was used for immunohistochemistry.

2.9. Lymphangiography of full length collecting vessels

21 days after control or FB-VEGF-C treatment, mice were anesthetized and 1 μl of anti-podoplanin (10 μg/ml) with FcγR blocking buffer, were injected intradermally from the dorsal side of the ear. 2 h later, 1 μl of secondary antibody Alexa Fluor® 594 conjugated (10 μg/ml) with FcγR blocking buffer were injected. Mice were euthanized by CO_2 and perfused with Ringer's buffer (described previously) and subsequently fixed with 2% paraformaldehyde. Hair from the back of fixed mouse was removed by depilation cream, washed well with water and 2 μl of FITC labeled 2000 kDa dextran (10 mg/ml) was injected in the dorsal side of the ear. By following the afferent collecting vessels under a fluorescence stereomicroscope, the ear pinna, ear canal, afferent lymphatics, auricular lymph node embedded in fat and neck dermis beneath were removed from the cadaver. The fat tissue surrounding the lymphatic vessels and lymph nodes was cleaned gently, and the complete lymphatic collecting vessels with the lymph node was imaged. Vessel diameter and valve morphology was measured under fully automated fluorescence stereo microscope (Leica M205 FA).

2.10. Interstitial flow-dependent lymphatic drainage assay

1% agarose (Ultrapure, Invitrogen) was prepared with distilled water and melted at high temperature. A series of 2 μl agarose droplets was applied on a parafilm sheet to solidify for about 10 min at 4 °C. After that, 10 μl of PBS with 5 mg/ml TRITC dextran (Sigma-Aldrich) was applied on top of each solidified agarose bead and albumin or dextran was allowed to equilibrate with agarose gel overnight at 4 °C in a humid chamber. The next day, free albumin solution was blotted with paper and beads were washed with PBS, and stored in a humid chamber at 4 °C. The same day, 21-day old ear skin flaps were cut along initial incision and lifted to expose the healed wound within the cartilage. A single albumin or dextran-loaded bead was placed on the top and at the center of the cartilage wound and ear flap was closed back and sealed with surgical glue. Using the stereomicroscope, the mean fluorescence intensity was measured at every 2 min for 1 h.

2.11. Intravital imaging of DCs migration and DC-lymphatic interaction

Intravital immunofluorescence labeling: The experimental procedure of intravital imaging is described elsewhere [38]. 21 days after, the control or FB-VEGF-C treated ventral dermis was cut vertically along antihelix pinna, and ventral dermis together with the cartilage was gently removed from dorsal skin. The tissue was cleared from blood clots using Ringer-Lactate buffered with 20 mM HEPES. Meanwhile, 10 μg/ml LYVE-1 (RELIAtech, San Pablo CA, USA), 10 μg/ml Collagen IV (Abcam, Cambridge, MA) in FcγR blocking solution was applied on the ear dermis for 15 min. The ear was washed well with ice-cold Ringer-Lactate buffer and 2 μg/ml donkey anti-rabbit Alexa Fluor 594 (Invitrogen) with FcγR blocking buffer was applied on the ear dermis for 15 min. *Preparation of dendritic cells*: Bone marrow cells were isolated from tibias and femurs from 8–12 weeks old eGFP/Balbc mice. Cells were matured for 7 days in RPMI 1640 supplemented with 10% fetal bovine serum (Gibco) and 50 μM 2-mercaptoethanol (Sigma-Aldrich) and 20 ng/ml GM-CSF (R&D Systems), and 15 h before imaging, DCs were activated with 200 ng/ml LPS (Sigma-Aldrich). The mature DCs (5×10^6 cells/ml in 100 μl) were pipetted onto the dorsal dermis and incubated for 30 min. Unattached cells were gently washed and drained with a sterile wipe. To prevent photobleaching, ascorbate-Ringer buffer [38] was constantly delivered (1 μl/min) with a peristaltic pump system where the needle outlet was placed 0.5 cm away from the ear. Body temperature was maintained with the heating pad and feedback rectal thermistor (DC Temperature Control System FHC Inc, Bowdoin MA, USA). Multiple regions were imaged for 6–12 h at 250× magnification with a motorized Leica fluorescent stereomicroscope (Leica M205 FA).

Quantification of DC migration to the lymph node: 8–12 week old eGFP Balb/c mice were sacrificed by CO_2. The spleen and lymph nodes were digested in a mixture of 2.5 mg/ml collagenase D and 50 U/ml DNase I (Sigma-Aldrich) for 30 min at 37 °C. Cells were then filtered with a 70 μM cell strainer (Fisher Scientific, Waltham, MA, USA) and washed with Hank's HBSS buffer supplemented with 0.5% bovine serum albumin and 5 mM EDTA. Cells were counted and for every 10^9 cells, 100 μl of $CD11c^+$ magnetic beads (Miltenyi Biotec, Bergisch Gladbach, Germany) was mixed with the solution for 15 min at 4 °C. Solution was washed from unbound magnetic beads and $CD11c^+$ cells were magnetically sorted using a magnetic column (Miltenyi Biotec). Isolated cells were then centrifuged and cell-fibrinogen mixtures were made by mixing 1×10^6 cells with 3 mg/ml fibrinogen, 2 U/ml thrombin, and 1 μg/ml LPS in 5 μl of volume. 21-day-old ear wounds, initially treated with control or FB-VEGF-C were surgically re-opened along the original wound cuts and ventral ear skin was lifted exposing healed tissues within the cartilage layer. For every wound area, 5 μl of cell-fibrinogen mixture was applied just after adding thrombin. The ear-flap was closed back and the edges of the wound were sealed with surgical glue. 18 h later, the mouse was sacrificed and the draining lymph node was harvested and analyzed by flow cytometry.

2.12. Diabetic full thickness skin wound healing

Mice were anesthetized with 3% isofluorane (Minrad Inc., Buffalo, NY) using a humidified delivery system, and maintained under 1.5% isofluorane during the procedure. The backs of 10–14 week old C57BLKS/J-m/Lepr db (*db/db*) mice were shaved and a 6 mm diameter biopsy punch (Stiefel, Middlesex, UK) was used to create a wound on the back of the mouse. 200 ng of VEGF-C, FB*-VEGF-C or FB_2-VEGF-C were mixed with 70 μl of hydrogel mixture (10 mg/ml human fibrinogen (Sigma), 2 U/ml thrombin (Sigma-Aldrich), 4 u/ml FXIIIa (CSL Behring), 25 μg/ml aprotinin (Roche Diagnostics), 5 mM $CaCl_2$) and these mixtures were immediately applied on the wounds. Wounds were covered with an adhesive film dressing (Hartmann, Heidenheim Germany). After 10 days, the animals were euthanized with CO_2, intracardially perfused and fixed with zinc fixative (4.5 Mm $CaCl_2$, 38 mM $ZnCl_2$, 38 mM $Zn(CF_3COO)_2$, 6 mM glycine, pH adjusted with NaOH to 6.5) modified after Kilarski et al. [38]. Wounds were used for histological analysis.

2.13. Histology and immunostaining

Diabetic full thickness wounds: The details of the analysis are explained elsewhere [39]. Briefly, wounds were excised in 8 mm diameter to include the margins, and vertically cut into two equal halves and embedded into the paraffin. Histological analysis was performed from 8 μm longitudinal wound sections and used for hematoxylin and eosin, Sirius red (picosirius red) immunofluorescence staining. H&E images were taken using a Slide Scanner VS120-L100 (Olympus, Volketswil, Switzerland).

Cartilage-replacement wound healing: Samples were incubated

in zinc fixative for at least 24 h at 4 °C. Ears were then washed with 1× TBS buffer at pH 7.5 and tissues were either embedded in paraffin and sectioned or the dorsal skin was peeled off from ventral dermis and whole mount stained. Primary antibodies: anti-Lyve-1 (RELIAtech), anti-podoplanin, anti-tenascin-C, anti-CCL21-biotin (R&D Systems) anti-collagen IV-biotin (Abcam, Cambridge, UK), anti-von Willebrand (Abcam), rabbit anti-αSMA (Abcam). Secondary antibodies; anti-rabbit Alexa Fluor®488, donkey anti-goat Alexa Fluor® 594 and streptavidin Alexa Fluor® 647 (Invitrogen), anti-rabbit Dy light®488 (Abcam) and 0.5% Casein in TBS was used for blocking buffer and staining for primary and secondary antibodies.

2.14. Flow cytometry

Only the wounded side of the ear dermis was used for the analysis. The dorsal and ventral ear skin layers were split into two separated tissues and digested in 10 mg/ml Collagenase IV and 50 U/ml DNAase for 45 min at 37 °C. Lymph nodes were digested in 1 mg/ml collagenase IV and 50 U/ml DNase followed by 3.3 mg/ml collagenase D [40]. Digested tissue was filtered through a 70 μM cell strainer and collected cells were stained for flow cytometry using fluorescently conjugated anti-CD45-biotin, anti-Podoplanin, anti-CD31, anti-CD3, anti-Ly6C, anti-CD11b, anti-CD11c, anti F4/80 (eBiosicence San Diego, CA), anti-Ly6G, anti-MHC II (Biolegend, San Diego, CA, USA), primary rabbit anti-Lyve-1 (RELIAtech, San Pablo CA, USA) and streptavidin Pacific Orange conjugate™, donkey anti rabbit Alexa Fluor® 647 (Invitrogen).

2.15. Image quantification

In vitro lymphangiogenesis: Images of the matrix and endothelial cells were collected using a laser scanning confocal microscope (Zeiss LSM 510, Heidelberg, Germany). The matrix was visualized using confocal reflectance, utilizing the reflective qualities of the collagen fibers under 633 nm laser illumination. Two sets of 25x 3-D image stacks that scanned a depth of 100 μm and a length of 1.46 mm were collected in each chamber. The number of multicellular organizations (minimum 3 nuclei) was counted. The volume, and the percentage of total cells in structure was calculated from 3D projections images using Imaris 7.1 (Bitplane, Zurich, Switzerland) algorithm. *In vivo lymphangiogenesis: S*ections were imaged using Leica SP5 white light laser confocal microscopy. 3D image stacks were analyzed using the algorithm from Imaris 7.1 Bit Plane software. Lyve-1 and Podoplanin threshold signals was adjusted and total area of positive pixels was normalized to total wound area. Tile images of diabetic wound sections were imaged using Zeiss Axioplan for image quantification, and Leica SP5 white light laser confocal microscopy was used to take representative images. An algorithm was created in Fiji software to select wound area in tile images and to omit artifact and autofluorescent staining. The number and area of each vessel was calculated together with the total Lyve-1 positive area per wound area. *Quantification of CCL21 staining:* Confocal images were taken using Zeiss LSM 710 confocal microscope. Images were taken from lymphangiogenic regions of the diabetic wound. 3D stack images were analyzed using Fiji software. The average mean intensity of each image was measured after signal thresholding. *Diabetic wound healing:* Re-epithelization and the thickness of the granulation tissue were measured on hematoxylin and eosin stained sections using Fiji. Images were converted to binary and the threshold set to count positive pixels in the granulation tissue. The distance between the panniculus carnosus under hypodermis was measured to estimate the initial wound diameter and the percentage of wound closure was calculated by measuring the diameter where re-epithelization was not yet formed. Complete re-epithelization was assumed as complete wound closure. The granulation tissue area between original wound margin (between panniculus carnosus, hypodermis and dermis) was measured.

2.16. Statistics

One-way ANOVA was used for multiple comparisons with Tukey's post-priori test. Unpaired Student's t-test was used to compare independent groups and paired Student's t-test was used when two different conditions were tested on the same animal. Differences were considered significant when $p < 0.05$. Samples were tested for normal distribution and groups for equal variance before running statistical test using Prism 5 (GraphPad, La Jolla, CA) Error bars show standard deviation. Each individual experiment was repeated at least two times. Samples were not excluded specifically from analysis and no randomization or blinding protocol was used. Sample size was sufficient to determine large statistical differences and compare the variance similarity between tested groups. Data meets the assumptions of the tests. Statistical test was not used to predetermine the sample size.

3. Results

3.1. FB-VEGF-C is stable in fibrin and released upon fibrin degradation

The design and expression of fibrin-binding protein variants has been described previously [32]. The transglutaminase substrate sequence α_2-PI_{1-8} links VEGF-C to fibrin during the thrombin/FXIIIa-mediated polymerization of soluble fibrinogen, which is cleaved during the proteolytic degradation of fibrin via plasmin. We constructed FB*-VEGF-C (i.e., α_2-PI_{1-8} -VEGF-C) and further fused an interpositional MMP substrate peptide [41] to engineer FB-VEGF-C (i.e., α_2-PI_{1-8}-MMP-VEGF-C) to provide dual enzymatic sensitivity for the proteolytic release of VEGF-C [41] (Fig. 1A). The α_2-PI_{1-8} or α_2-PI_{1-8} −MMP substrate domain is fused to the N-terminal side of VEGF-C (Supplementary Fig. 1) and increases the molecular weight of monomers of mature VEGF-C, as shown by SDS-PAGE gels stained with Simply Blue SafeStain (Fig. 1B).

To test the bioactivity of the engineered proteins, LECs were stimulated with VEGF-C variants for 5, 10 and 15 min. Surprisingly, both FB*-VEGF-C and FB-VEGF-C variants induced stronger and time-dependent VEGFR-3 phosphorylation compared to commercially available wild-type VEGF-C (Fig. 1C). Notably, the same concentrations of wild-type and fibrin-binding forms of VEGF-Cs similarly increased the proliferation of LECs after 24 h of incubation (Fig. 1D).

To assess the functionality of the α_2-PI_{1-8} domain in immobilizing VEGF-C to fibrin and the requirement of proteolysis for its release, we prepared fibrin gels with FB-VEGF-C and measured the release of VEGF-C over 3 days under protease-free conditions. After an initial 20% release of unbound FB-VEGF-C, the remaining FB-VEGF-C was not released in the plasmin-free conditions; in contrast, more than 80% of wild-type VEGF-C was released within 3 days. We demonstrated a plasmin-mediated release over several days, with a linear release of VEGF-C with simulatenous fibrin degradation (Supplementary Fig. 2). We also showed that FB-VEGF-C binds to fibrin spontaneously deposited in the injured tissues (without using a hydrogel implant, Supplementary Fig. 3).

To visualize the release of VEGF-C *in vivo*, we used fibrin gels with fluorescently labeled VEGF-C variants, which was implanted in the skin of both sides of the back of BALB/c mice. The cumulative infrared fluorescence showed that more than half of the wild-type VEGF-C was released within 3 days and none could be detected at 8

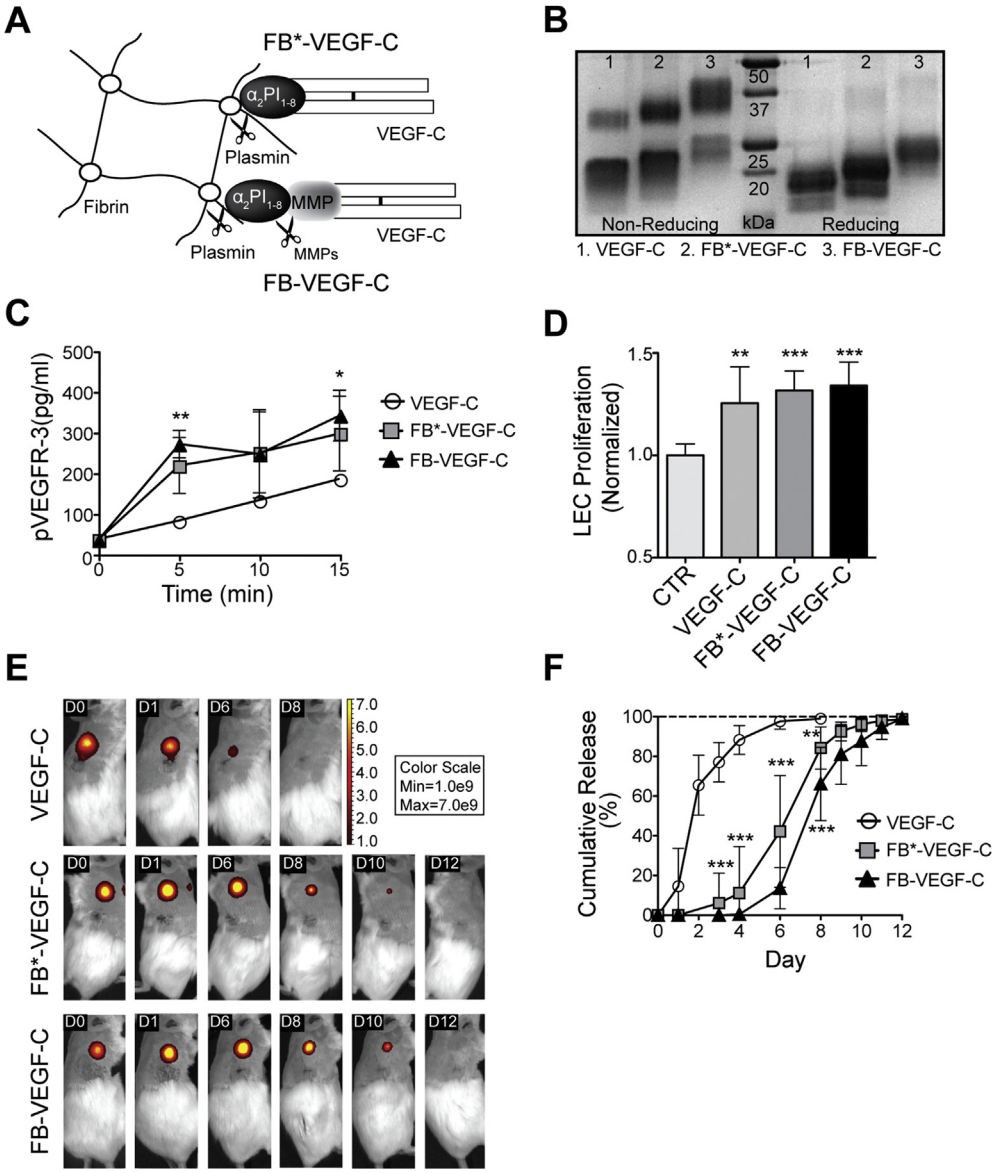

Fig. 1. Bioactivity and extended delivery of fibrin-binding VEGF-C variant. **A,** The mature form of VEGF-C was fused with the peptide α_2-PI_{1-8}, a substrate for FXIIIa during the formation of insoluble fibrin clots. VEGF-C release was enabled by plasmin cleavage of fibrin or MMP cleavage of the additional MMP substrate peptide fused between the α_2-PI_{1-8} domain and VEGF-C. **B**, SDS-PAGE gels of wild-type VEGF-C (1); FB*-VEGF-C (lacking the MMP cleavage domain) (2); and FB-VEGF-C (containing it) (3) under non-reducing and reducing conditions. **C**, VEGFR-3 phosphorylation (pVEGFR-3) as measured by enzyme-linked immunosorbent assay (ELISA) after stimulating lymphatic endothelial cells (LECs) with 100 ng/ml free or fibrin-binding forms of VEGF-C for 5, 10 and 15 min ($n \geq 3$). **D**, LEC proliferation by Alamar Blue assay after 24 h treatment with 100 ng/ml free or fibrin-bound forms of VEGF-C, relative to untreated control group ($n = 7$). **E,** In vivo maintenance of FB-VEGF-C variants implanted in fibrin over 10 days. 1 μg fluorescent dye was conjugated to wild-type VEGF-C, FB*-VEGF-C or FB-VEGF-C and implanted subcutaneously in fibrin, and measured by infrared spectrometry. Representative images show the radiant efficiency ($[p/s/cm^2/sr]/[\mu W/cm^2]$) of the fluorescent VEGF-C in the gels. **F,** Cumulative release VEGF-C from *in vivo* imaging data ($n \geq 3$, mean ± SD) $^*p < 0.05$, $^{**}p < 0.01$, $^{***}p < 0.001$. (For interpretation of the references to colour in this figure legend, the reader is referred to the web version of this article.)

days (Fig. 1E and F). FB*-VEGF-C and FB-VEGF-C release started 6 days later than that of wild-type VEGF-C, and the process was completed in 12 days. No difference was detected between the release of FB*-VEGF-C and FB-VEGF-C. Thus, the incorporation of a fibrin-binding sequence within VEGF-C resulted in sustained binding and prolonged release from a fibrin-based biodegradable matrix.

3.2. FB-VEGF-C variants induce in vitro lymphatic capillary formation with interstitial flow synergistically

Because the VEGF-C engineering strategy could diminish the need for the repeated administration of VEGF-C, we investigated if a single dose of VEGF-C embedded in fibrin could promote lymphangiogenesis in vitro. We incorporated wild-type VEGF-C, FB*-VEGF-C or FB-VEGF-C in a fibrin gel and allowed LECs to grow for 6 days in a radial flow chamber. Slow interstitial flow has been shown to guide capillary and lumen formation by promoting the endothelial cell sensing of growth factor gradients in the surrounding environment [42]. Indeed, applying flow within 3D gels drastically modulated the effect of both FB*-VEGF-C and FB-VEGF-C on lymphatic capillary formation compared to the wild-type form of VEGF-C (Fig. 2A). We did not find any difference between FB*-VEGF-C and FB-VEGF-C, as both types similarly increased the ratio of cell volume in the gel and the number of cells in the structures (>3 cells) (Fig. 2B–C, Supplementary Fig. 4). Lymphatic capillaries formed

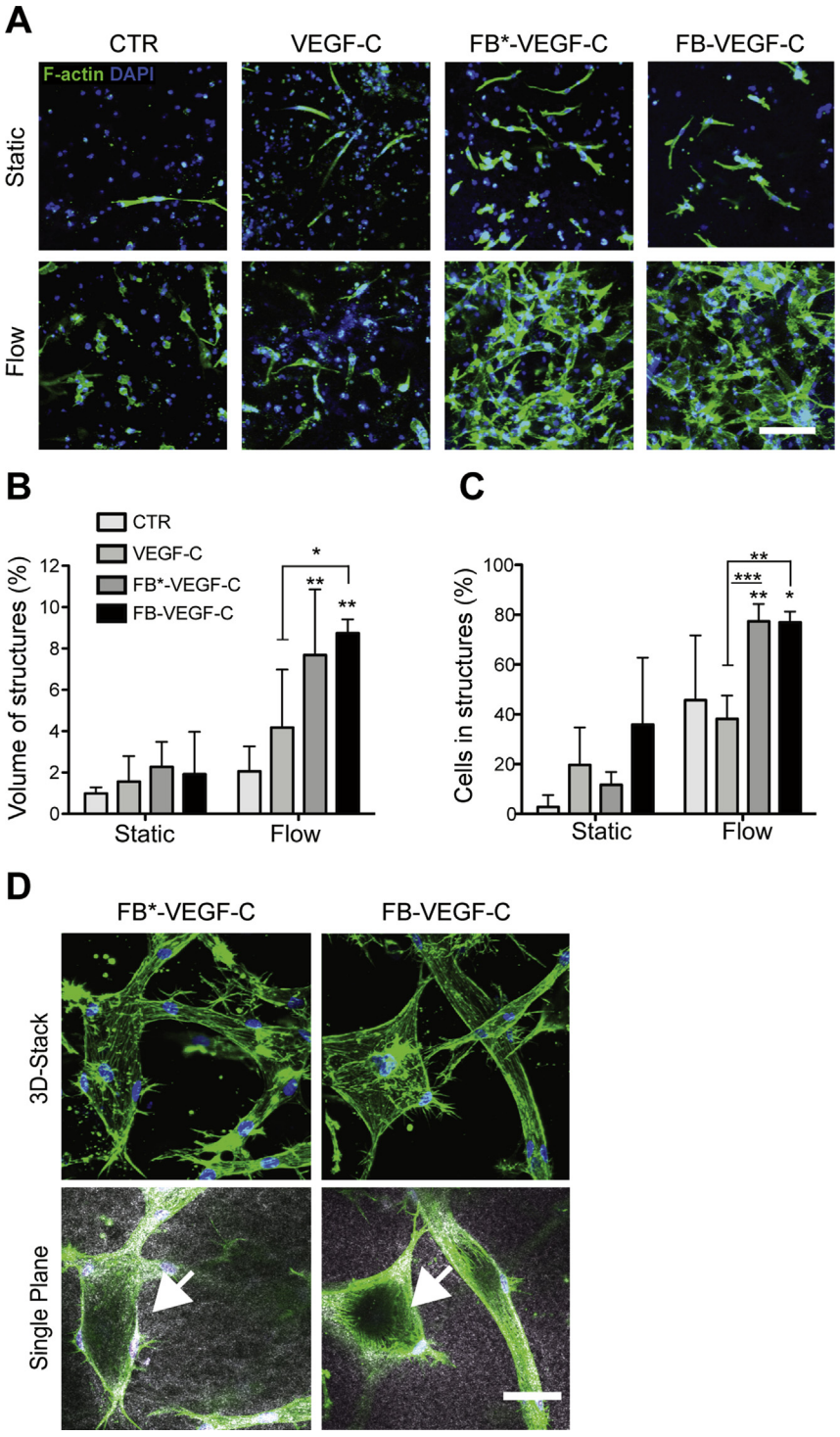

Fig. 2. Fibrin-binding VEGF-C variants act synergistically with interstitial flow to drive lymphatic capillary morphogenesis in vitro. **A**, Representative confocal images show capillary formation of lymphatic endothelial cells (LECs) after 6 days of 3D culture in fibrin with 100 ng/ml wild-type VEGF-C, FB*-VEGF-C or FB-VEGF-C, under static or flow (1 μm/s) conditions (Scale bar: 100 μm). Quantification of capillary formation is shown by (**B**) percent volume of LECs in the 3D matrix and (**C**) numbers of cells forming structures (incorporation of ≥3 nuclei) counted from 25× z-stack images (n = 3, mean ± SD). **D**, Confocal z-stack and single-plane confocal reflectance images of extracellular matrix fibers show lumen (arrows) within newly formed lymphatic capillaries. (green: F-actin, blue: DAPI, grey: fibrin; scale bar:50 μm) $^{*}p < 0.05$, $^{**}p < 0.01$, $^{***}p < 0.001$.

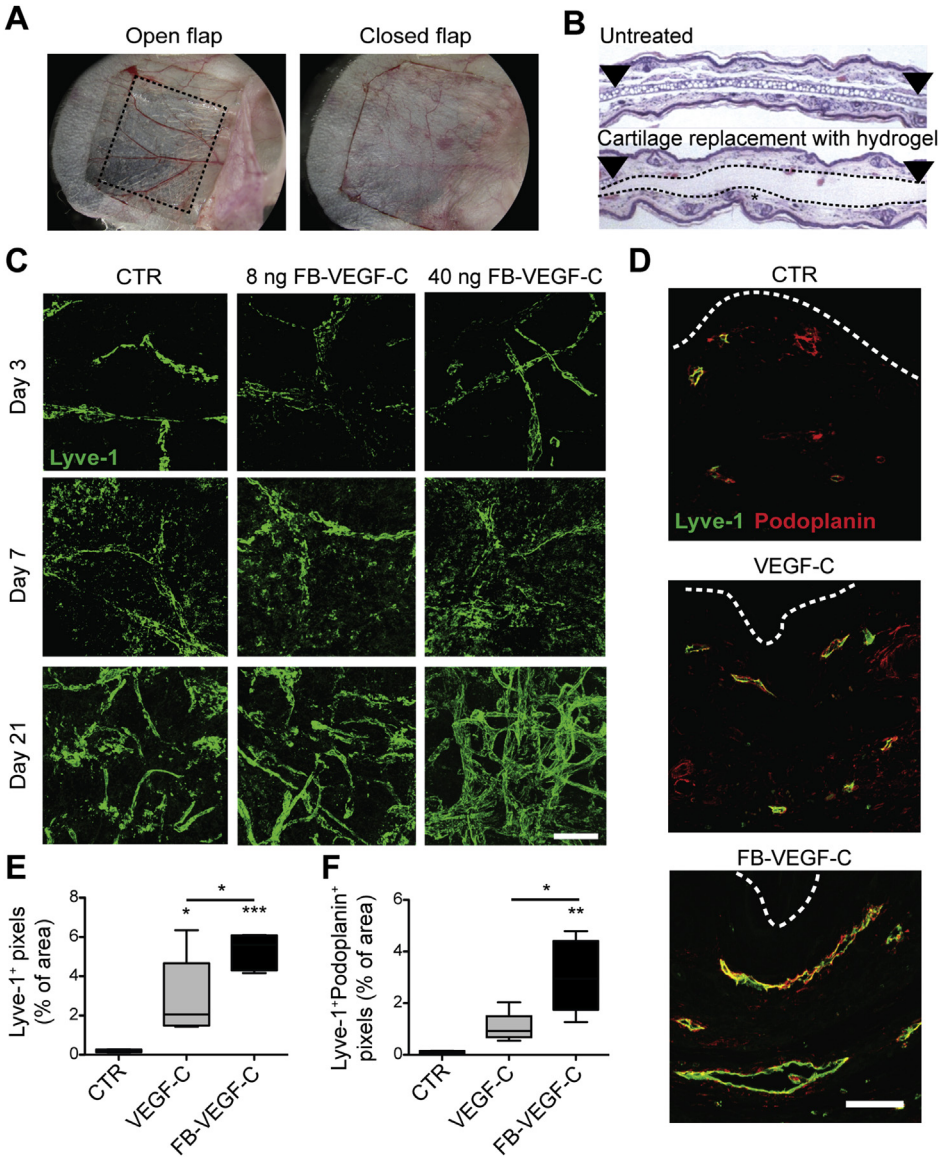

Fig. 3. Fibrin-binding VEGF-C implanted in the ear promotes lymphatic capillary hyperplasia. **A,** Illustration of the surgical procedure of the ear. After the surgical cut is made, the cartilage is removed, and the hydrogel is implanted into the central part. The ear-flap is then closed, and the skin edges are sealed with surgical glue. **B,** Hematoxylin and eosin staining of untreated and gel-implanted ear sections. In (A) and (B), the dotted line shows the gel-implanted area and the borders where the cartilage was removed. **C**, Confocal images show the lymphatic vessels labeled with Lyve-1 (green) by whole mount immunostaining of the dorsal ear skin. Control, 8 ng and 40 ng FB-VEGF-C in a hydrogel applied to the wound. Representative images show the whole mount staining 3, 7 and 21 days after wound healing (Scale bar: 100 μm). **D,** Immunostaining of the ear tissue 21 days after the application of the control, wild-type VEGF-C or FB-VEGF-C gel. Paraffin-embedded tissues sectioned at 5 μm thickness and stained with podoplanin (red) and Lyve-1 (green) (Scale bar:100 μm). Dashed borders show the ear epithelium. **E,** Lyve-1-positive and (**F**) Lyve-1 podoplanin-positive percentage areas were calculated for each ear wound area ($n \geq 4$, $^{*}p < 0.05$, $^{**}p < 0.01$, $^{***}p < 0.001$).

lumens, as shown in a single-plane confocal microscopy image (Fig. 2D, Supplementary Fig. 5). Lumen formation was previously shown to be an indicator for biophysically stable and functional endothelial cell structures that are able to transfer fluid [43]. Because the release rates of FB*-VEGF-C and FB-VEGF-C were similar, we concluded that the release was governed by the same plasmin-dependent release mechanism. Because these two proteins also displayed similar bioactivity, we decided to use only FB-VEGF-C to further test the effect of matrix-immobilized VEGF-C on *in vivo* lymphangiogenesis.

3.3. FB-VEGF-C induces remodeling in lymphatic capillaries but not in downstream collecting vessels

Next, we tested the local effect of FB-VEGF-C in a subcutaneous cartilage-replacement healing model *in vivo* (Fig. 3A). Histological sections of day 0 wounds showed fibrin gel filling the gap after the cartilage excision (Fig. 3B). Before comparing the effect of wild-type and FB-VEGF-C, we determined the optimum dose (40 ng) and time (21 days) to induce extensive lymphangiogenesis (Fig. 3C). Cross sections of the control and the wild-type VEGF-C- and FB-VEGF-C-treated ears confirmed that by 21 days after wounding, extensive lymphangiogenesis was induced in FB-VEGF-C-treated wounds, but not in control gel or wild-type VEGF-C-treated wounds (Fig. 3D–F). We showed that FB-VEGF-C had no effect on morphology of growing blood vessels as characteristic hyperplastic abnormalities like micro aneurysms or tortuosity [44,45] were not detected. Despite invasive presence of hyperplastic lymphatics, newly formed blood vessels had uniform diameter and basement membrane support similar to blood vessels in control wounds

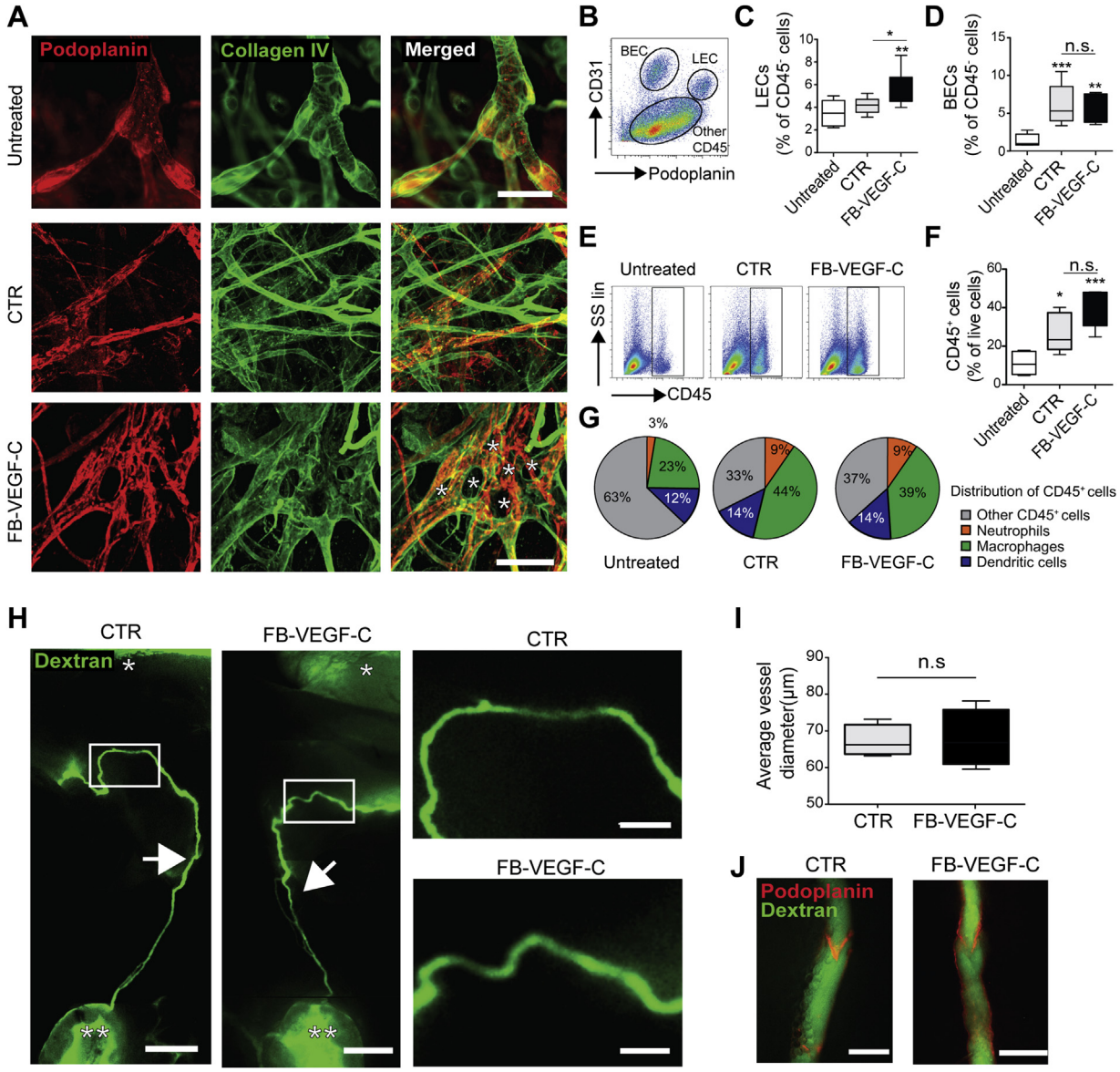

Fig. 4. Lymphangiogenic gels induce local lymphatic hyperplasia but do not remodel downstream collecting vessels. **A,** Whole mount confocal images of untreated dorsal ear dermis and 21 days after treatment with the fibrin gel control (CTR) or FB-VEGF-C. Images show podoplanin (red) and collagen IV (green) staining. Stars indicate pillar formation on the FB-VEGF-C-treated condition (Scale bar: 50 μm). **B,** Representative flow cytometry plot showing the gating strategy of LECs; podoplanin$^+$CD31$^+$, BEC; CD31$^+$podoplanin$^-$, and other CD45$^-$ cells in the skin. The ratio of LECs (**C**) and (**D**) BECs among total CD45$^-$ cells. (**E**) Representative flow cytometry graphs of CD45$^+$ cells in healthy, control and FB-VEGF-C-treated wounds after 21 days. (**F**) The ratio of CD45$^+$ cells in the gel implanted area. (**G**) Pie chart showing neutrophils (Ly6G$^+$CD11b$^+$), macrophages (F4/80$^+$CD11b$^+$), DCs (MHCII$^+$CD11c$^+$), and other CD45$^+$ cells in untreated, control or FB-VEGF-C-treated conditions ($n \geq 5$). (**H**) Zoomed out image of the fixed ear after the injection of FITC-dextran. *ear anti-helix pinna, **auricular lymph node, and the arrow shows afferent lymphatic vessels. (Tile image scale bar: 800 μm, zoomed in picture: 200 μm) (**I**) Average vessel diameter measured by taking the average of 10–15 measurements between the antihelix pinna to the draining lymph node. Images were taken under stereomicroscopy. (**J**) Intravital labeling of collecting lymphatic vessels draining the lymphangiogenic site (dextran, green) with valves shown (podoplanin, red). Scale bar: 75 μm; $n = 4$, *$p < 0.05$, **$p < 0.01$, ***$p < 0.001$.

(Supplementary Fig. 6).

Whole-mount immunostaining of the subcutaneous wounds and untreated skin showed that extensive lymphangiogenesis induced pillar formation and intussusception, forming large diameter vessels compared to control gel wounds. This result is consistent with features described for vascular hyperplasia [46] (Fig. 4A). Healed wounds were also analyzed by flow cytometry. We confirmed that the LEC population increased after FB-VEGF-C treatment (Fig. 4B–C), while the treatment did not affect blood endothelial cells (BECs) (Fig. 4D) or other CD45$^-$ cells (Supplementary Fig. 7). In addition, the expected increases in leukocyte, neutrophil and macrophage infiltration were not affected by FB-VEGF-C (Fig. 4E–F), as well as activated DCs (Fig. 4G, Supplementary Fig. 8). These results showed that FB-VEGF-C had a local effect only on LECs at 21 days after its administration.

Next, we tested whether locally administered FB-VEGF-C affects the morphology of downstream collecting vessels. We used post-mortem, fixed, intact tissue to visualize the morphology of collecting vessels between antihelix pinna to auricular lymph node. Fluorescence lymphangiography revealed that the downstream collecting vessels did not show obvious evidence of remodeling with regards to lymphatic sprouts and morphological abnormalities at the valve locations (Fig. 4H–J). These results showed that FB-VEGF-C induced only local effects on lymphatics and 21 days

after its administration, no alteration in the local immune infiltration was detected.

3.4. Fluid clearance is unaltered by local lymphangiogenesis

We investigated the fluid and solute transport capability of lymphangiogenic vessels with a new clearance assay. We designed this method to avoid the effects of injection pressure on lymphatic clearance (Supplementary Fig. 9), which is typically encountered in clearance assays. Instead, the clearance of fluorescence dextran implanted on the exposed dermis relied on diffusive and convective forces driven entirely by the dynamics of tissue blood and lymphatic circulations. To demonstrate that lymphatic abnormalities in collecting vessels can be detected by the implantation technique, we tested a control case where lymphatic collecting vessels were blocked by anti-lymphatic photodynamic therapy, a technique that specifically occludes lymphatic collecting vessels but not lymphatic capillary or blood vessels [47]. Indeed, we found lymphatic occlusion resulted in complete inhibition of dextran clearance from the skin (Supplementary Fig. 10). Next we tested the drainage of microbeads implanted under the ventral skin-flap that had been treated with control or FB-VEGF-C hydrogels (Fig. 5A–C). Interestingly, no differences in clearance rates were observed between the control, control wound, or hyperplastic lymphatics (Fig. 5D).

3.5. DC emigration is enhanced in lymphangiogenic regions

The effect of FB-VEGF-C-induced lymphangiogenesis on DC migration was visualized by intravital immunofluorescence imaging, a technique that has been previously used in our laboratory to visualize leukocyte vessel transmigration [38,48]. First, we verified that DCs, isolated from eGFP BALB/c mice, were attracted to both control and hyperplastic lymphatics of the wound and migrated towards lymphatic vessels for 7 h. This indicated that both vessel types could support major transmigratory immune functions for normal lymphatic vessels (Fig. 6A and Supplementary Videos 1 and 2). Next, we investigated DC trafficking to the lymph node, avoiding potential unwanted effects of direct injection (e.g., into lymphatic vessels or increased local interstitial pressure) by implanting the DCs directly onto control or FB-VEGF-C-treated wounds. We found substantially increased DC homing to the draining lymph node from lymphatic hyperplastic regions than from control wounds (Fig. 6B–C). In contrast to the DCs that remained in the ear, the DCs that migrated to the lymph node showed a mature phenotype ($CD86^{+}MHCII^{+}$) (Fig. 6D).

Supplementary data related to this article can be found online at http://dx.doi.org/10.1016/j.biomaterials.2017.03.033.

3.6. FB-VEGF-C promotes diabetic wound healing

In healthy wounds, FB-VEGF-C induced extensive lymphangiogenesis and increased immune cell trafficking. To determine the therapeutic effect of FB-VEGF-C, we used a mouse model of type II diabetes mellitus (db/db mice), where poor vascularization is one of the reasons for impaired tissue healing, as a model of chronic wounds [49]. Fibrin hydrogels containing control, VEGF-C, or FB-VEGF-C were implanted on back skin wounds according to our previously published protocol [39]. As a positive healing response parameter, we measured the thickness of the GT that formed within the wound and wound re-epithelialization (Supplementary Fig. 11). Notably, this is an approximately 500-fold lower dose than what has been used in previous studies [21,50]. GT thickness reflects wound vascularization and also the degree to which transient fibrin is replaced with fibrous, contractile tissue populated with macrophages and myofibroblasts, cells critical for the deposition of new matrix components and subsequent wound closure [6]. We found that FB-VEGF-C increased GT thickness compared to the wild-type

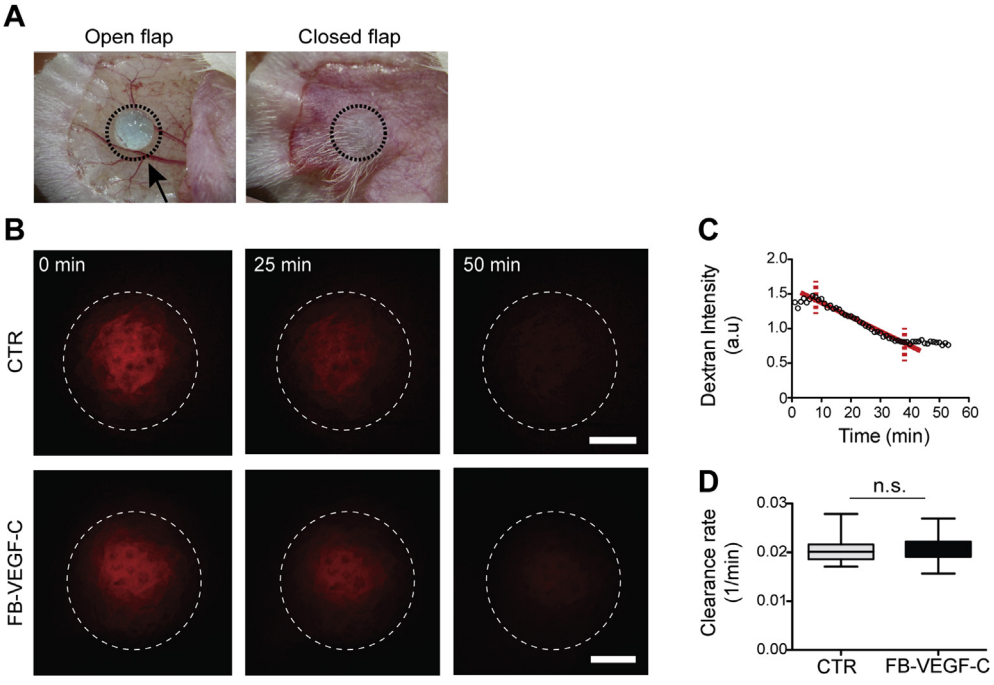

Fig. 5. Lymphatic clearance is unaltered by lymphangiogenic hyperplasia. A, Drainage assay: fluorescent dextran-loaded agarose beads were placed atop the lymphangiogenic region, and the ear skin flap was gently closed and sealed. **B,** Drainage was measured by tracking the fluorescence decay of 5 mg/ml 155 kDa TRITC dextran in 2 μl of 1% agarose beads every 2 min using a stereomicroscope (Scale bar: 1 mm). **C,** Representative graph of dextran intensity decay over time. Red line shows the time frame when the clearance rate was linear and the slope of the intensity was measured. **D,** The clearance rate (1/min) was calculated using the slope of the intensity over time (n = 7). (For interpretation of the references to colour in this figure legend, the reader is referred to the web version of this article.)

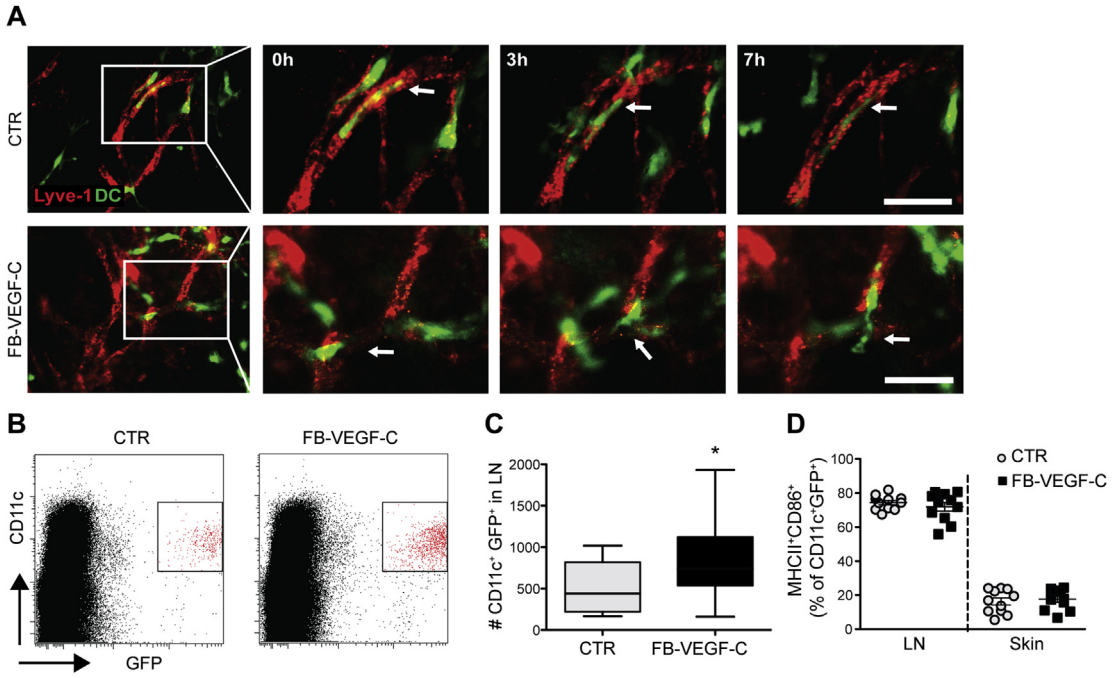

Fig. 6. Engineered lymphangiogenesis enhances the local migration of activated DCs. A, Intravital microscopy imaging of dermal lymphatics (LYVE-1$^+$, red) and mature dendritic cells (DCs, eGFP$^+$, green) that had been placed on the wound. Arrows show DCs entering the newly formed lymphatic capillaries (Scale bar: 50 μm). **B,** Representative flow cytometry graph showing migrated DCs in the lymph node. **C,** Quantification of the total numbers of migrated DCs in lymph nodes draining the control vs. FB-VEGF-C-fibrin regions. **D,** The percent of activated DCs (CD11c$^+$MHCII$^+$CD86$^+$) among live GFP$^+$CD11c$^+$ cells in the lymph node and ear (n = 11, *p < 0.05).

VEGF-C and control groups, although wound re-epithelialization was not different (Fig. 7A–C). Lyve-1 and podoplanin-stained cross-sections of wounds showed that FB-VEGF-C also induced lymphatic hyperplasia in GT compared to the control and wild-type VEGF-C (Fig. 7D). The number of Lyve-1$^+$ vessels was remarkably increased by FB-VEGF-C, with more vessels per wound and more large-area (more than 1200 μm^2) vessels compared to that of wild-type VEGF-C and control groups (Fig. 7E–G). In addition, the deposition of collagen type I, collagen type III and tenascin-C at the border of large lymphatic vessels (Supplementary Fig. 12) might be associated with thick GT in FB-VEGF-C-treated wounds.

3.7. FB-VEGF-C enhances CCL21 and leukocyte trafficking in diabetic wounds

Lymphatics secrete chemokines that attract migratory leukocytes, DCs and neutrophils to the lymphatic vessel lumen [51,52]. We found that the total number of CD45$^+$ cells was not different in hyperplastic vessels compared to control vessels, but rather that more leukocytes were located within the lymphatic lumen of hyperplastic vessels and were frequently attached to the basolateral wall (Fig. 8A–D). The increased numbers of transmigrating leukocytes could be attributed to increased secretion of CCL21, a leukocyte chemoattractant, by VEGF-C-stimulated lymphatic endothelial cells [53]. In fact, we found that CCL21 expression by LECs was increased in regions of extensive lymphangiogenesis (Fig. 8E–F).

4. Discussion

Here, we developed a clinically suitable FB-VEGF-C delivery method via proteolytic plasmin or MMP cleavage and showed that increased lymphangiogenesis was restricted to the local initial lymphatic capillary bed. Using a system previously established in our lab [29,37,54], fibrin-binding forms of engineered VEGF-C are slowly released *in situ* from a provisional matrix, becoming accessible only to infiltrating cells [55,56]. A loss of bioactivity is a major obstacle when engineering functional proteins; however, we showed that the receptor-stimulating potential of modified VEGF-Cs was not affected. While low doses of wild-type VEGF-C had no biological effect *in vivo*, the administration of FB-VEGF-C induced lymphatic overgrowth within the initial lymphatic compartment, while the collecting vessels remained morphologically unaffected along its entire route to the draining lymph node.

In our study, engineered FB-VEGF-C was released as a function of fibrin degradation and remodeling over a course of 10–12 days, which is similar to the duration of the initiation of physiological lymphangiogenesis in wound healing [57], and this enables specific targeting of lymphatics without causing the remodeling of downstream vessels. Nevertheless, a physiological assay should test the functionality of the entire lymphatic network, independent of the correct morphology of the collecting vessels.

Fluorescence lymphangiography measures lymphatic clearance with a pressurized interstitial fluid injection, which, over short distances, might overestimate the maximum capacity of the lymphatic system. This is due to the abnormally high hydrostatic force generated within the tissue that is manifested by transient skin expansion (local mechanical edema) following intradermal injection. In addition, the high pressure at the needle outlet would alter the lymphatic clearance rate by influencing the transmural flow-dependent stroke volume per lymphangion [58]. Essentially, in small animals, such as mice, lymphangiography can be used to define the routes taken by functional lymphatic collecting vessels, but not to determine the drainage kinetics. The only method designed to quantify lymphatic drainage across the physiological pressure range in mice is the measure of lymphatic conductance specifically in tail lymphatics [59]. However, wounding of the tail skin also disrupts the collecting lymphatics [60] therefore, this approach does not represent regular skin healing. These

methodological limitations led us to develop an assay that aimed to detect any decline in lymphatic drainage capacity below the physiological influx level of the tissue interstitial fluid. To avoid pressurized fluid injection, fluorescent dextran loaded in agarose beads was implanted over the healed vasculature and subsequently delivered to the interstitium by interstitial fluid flow-dependent convection. A similar experiment on the ear with lymphatic collectors blocked by photo ablation showed that fluorescence evanescence was almost entirely dependent on the active lymphatic drainage. Because we compared the fluid drainage at physiological, rather than injection-enforced or edema-driven pressures, the lymphatic system could not be artificially overloaded and drained at its physiological pace. Any bottleneck capable of interfering with lymphatic flow should result in a delayed clearance of fluorescence. Using this method, we found no difference in the drainage between normal wound lymphatics and hyperplastic initial vessels from FB-VEGF-C stimulated wounds, substantiating that one of the most critical physiological functions of lymphatics was not disturbed by hyperplastic-like extensive lymphangiogenesis in the initial compartments of lymphatics.

Initial lymphatics, which form the entry routes for DCs, have an incomplete, thin basement membrane, and button-like junctions between endothelial cells are part of the primary valves that facilitate an influx of fluid [61,62]. Large, blunt-ended initial lymphatics are also morphologically quite different from collecting vessels, which are additionally supported by a full-thickness basement membrane and smooth muscle cells. This is in contrast to inflammation-induced, hyperplastic or lymphangiogenic capillaries, where button-like junctions (permeable) are replaced with continued zipper-like junctions (non-permeable) that are normally formed between the endothelium of collecting vessels [63,64]. Because button-to-zipper junction transformations during inflammation are VEGF-C-independent, we expected that the newly formed initial lymphatics would be capable of supporting leukocyte transmigration. Indeed, our intravital imaging designed to image lymphatic-DC interactions indicated that the morphological differences between normal wound and wound hyperplastic lymphatics had no effect on the basic function of initial lymphatics, allowing cells to squeeze between vessel walls and enter the new lymphatics of control wounds and hyperplastic vessels.

FB-VEGF-C-stimulated lymphatic capillaries displayed expanded lumens and larger vessel diameters, implying that more lymphatic surface area was available to the DCs to transmigrate in addition to the increased chemoattractant CCL21. Importantly, implanting DCs onto the remodeled tissue, rather than injecting them subcutaneously, guaranteed that the cells could use physiologically defined routes for tissue egress. Thus, we conclude that lymphatic hyperplasia leads to increased attraction and transmigration of immune cells but does not necessarily alter fluid or solute clearance *per se*.

In diabetic wounds, poor blood circulation results in the inadequate presence of growth factors in the healing environment, which eventually leads to diminished blood and lymphatic revascularization and is associated with increased edema and impaired wound healing [65]. FB-VEGF-C caused extensive lymphangiogenesis, which correlated with the formation of thicker GT in diabetic wounds. In a subcutaneous cartilage-replacement healing model, FB-VEGF-C increased only the number of lymphatic endothelial cells of initial lymphatics in the GT and had no effect on the density and morphology of blood vessels and macrophages as compared to the control wound. This mechanism is different from the VEGF-C effect reported by Saaristo et al. [20], where genetic overexpression of VEGF-C led to the equal stimulation of lymphatic and blood vessel growth and also attracted more macrophages that also expressed VEGFR-3. These authors concluded that stimulated blood angiogenesis and positive feedback from immigrated macrophages were the main factors leading to enhanced GT formation. In our model, however, FB-VEGF-C was administered at a low dose, and the bioavailability of the active growth factor was further restricted by a slow-release mechanism of VEGF-C from the matrix; this can explain its exclusive stimulation of lymphangiogenesis without blood vessel angiogenesis, as VEGF-C acts primary on lymphatic VEGFR-3. Regardless of the mechanism, only initial lymphatics responded to FB-VEGF-C stimulation; hence, they were likely responsible for the enhanced granulation tissue formation in diabetic wounds.

Impaired wound healing in diabetes is also associated with the persistence of pro-inflammatory leukocytes in wounds because of a high level of chemokine secretion [66] and possibly poor lymphatic vascularization that interferes with leukocyte evacuation. We found that the overall number of $CD45^+$ cells in diabetic wounds with induced extensive lymphangiogenesis did not change; however, more leukocytes were associated with the hyperplastic lymphatic vessels compared to normal vessels. In the skin, mature DCs and Langerhans cells express the CCL21 receptor CCR7, and are therefore chemoattracted to CCL21-secreting lymphatic vessels [1,67], which again is upregulated by VEGF-C [53]. Consistently, we found that hyperplastic lymphatic capillaries of diabetic wounds produced more CCL21 overall, which could explain the elevated leukocyte trafficking to the lymphatics, since equal numbers of leukocytes were found in FB-VEGF-C-fibrin-treated diabetic wounds compared to control wounds. This could suggest that increased CCL21 together with increased lymphatic surface area may be associated with the accelerated transmigration of leukocytes to lymph nodes. However, in addition to CCL21, the expression of other factors such as CCL2, CCL5, CCL20 as well as leukocyte adhesion receptors may affect this process [68].

Hyperplastic growth, or the enlargement of pre-existing vessels, has been previously induced with administration of direct and high doses of VEGF-C or in VEGF-C-overexpressing systems [55,56,69]. In collecting vessels, VEGF-C-induced hyperplasia cause malformations of collecting valves [19] [26,69] or vessel hyperpermeability [19,70] that are the primary causes of major pathologies of collecting vessels, slow or multi-directional drainage pattern and lymphatic blockage of DC trafficking. And even though these hyperplastic lymphatic vessels can normalize and gradually acquire hallmarks of mature collecting vessels [19] this process is slow and in certain conditions lymphatic hyperplastic vessels persist indefinitely [71], leading to lymphedema [72] In contrast, a low and single dose of fibrin-binding VEGF-C, induced local, functional lymphangiogenesis, which promoted immune cell emigration to the lymph node, in turn improving wound healing. FB-VEGF-C was released from fibrin by action of proteases produced by gel infiltrating cells and its gradual dosing had no effect on blood vessels or macrophages. Instead, FB-VEGF-C induced LEC proliferation only in capillaries but not collecting vessels that increased immune cell trafficking without affecting macromolecule drainage. This finding indicates that in contrast to lymphatic collectors, hyperplasia within initial compartment is beneficial for lymphatic functionality. This might be due to vastly distinct biomechanical functions of these two compartments as fluid drainage, leukocyte attraction and subsequent intravasation that occur at the level of cell or cell junctions, are independent and thus tolerant to morphological changes of the whole structure of initial lymphatic vessels. Lymphatic collectors however, cannot endorse similar plasticity as efficient unidirectional lymph transportation demands higher order co-operation in formation of multicellular valves. These results highlight the importance of

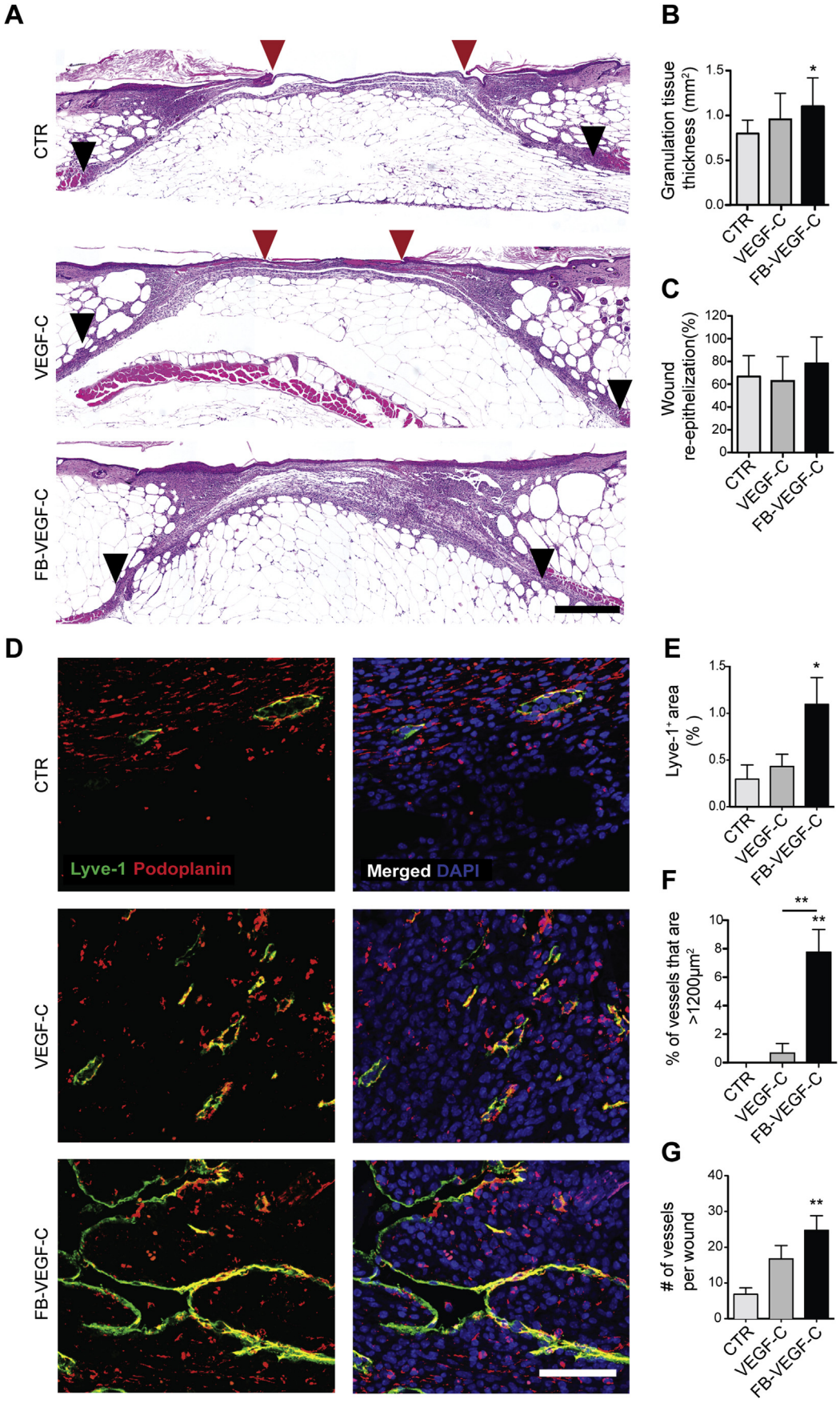
A
CTR
VEGF-C
FB-VEGF-C
B
Granulation tissue thickness (mm²)
1.5
1.0
0.5
0.0
*
CTR
VEGF-C
FB-VEGF-C
C
Wound re-epithelization(%)
120
100
80
60
40
20
0
CTR
VEGF-C
FB-VEGF-C
D
CTR
Lyve-1 Podoplanin
Merged DAPI
VEGF-C
FB-VEGF-C
E
Lyve-1⁺ area (%)
1.5
1.0
0.5
0.0
*
CTR
VEGF-C
FB-VEGF-C
F
% of vessels that are >1200µm²
10
8
6
4
2
0
**
**
CTR
VEGF-C
FB-VEGF-C
G
# of vessels per wound
40
30
20
10
0
**
CTR
VEGF-C
FB-VEGF-C

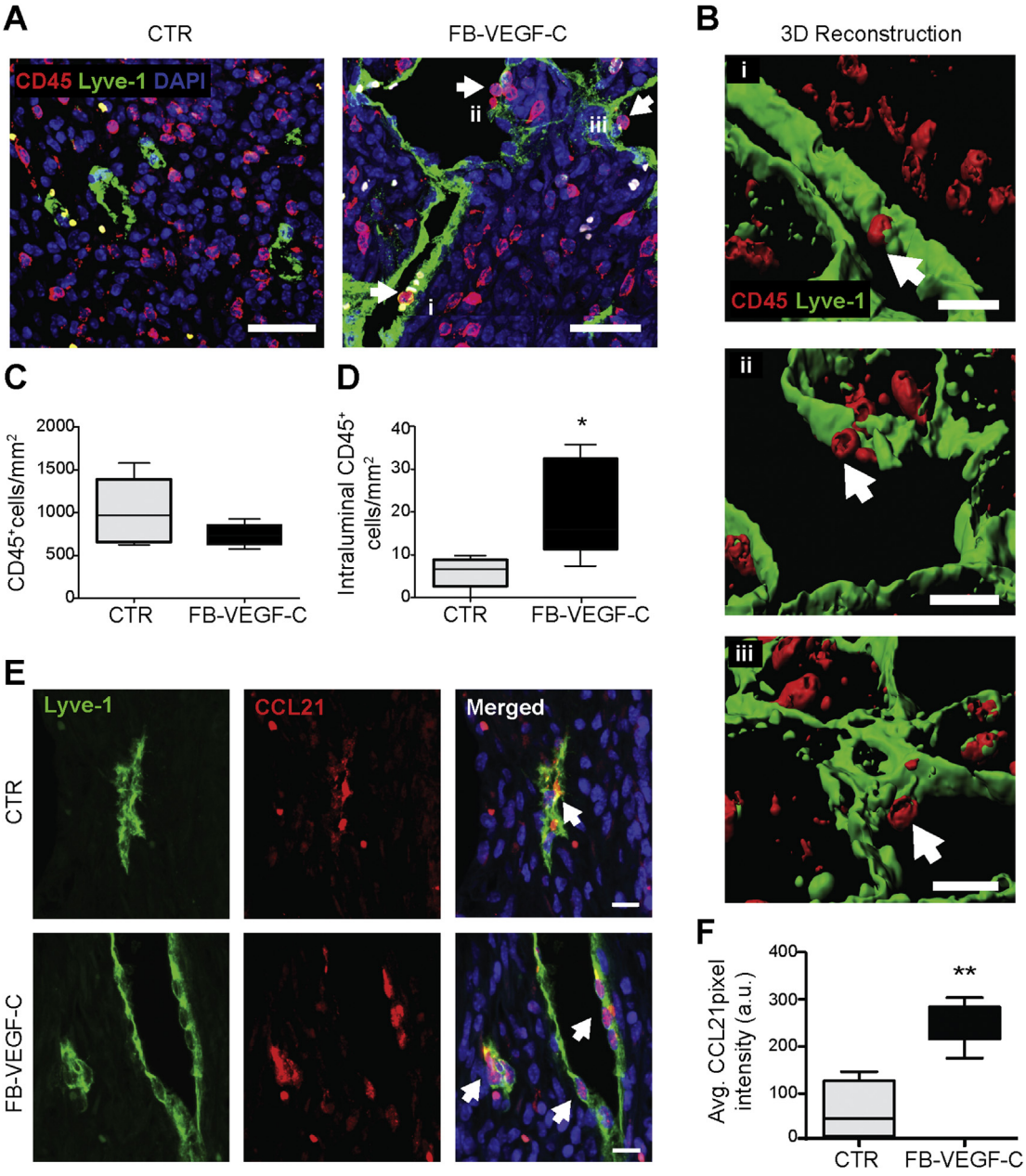

Fig. 8. Lymphangiogenic gels in diabetic wounds promote leukocyte interactions with lymphatic vessels through increased CCL21 expression. **A**, Paraffin-sectioned diabetic skin wounds were stained for CD45 (red), Lyve-1 (green) and DAPI (blue). The arrow shows $CD45^+$ cells staining for Lyve-1^+ in the lymphatic lumen (Scale bar: 30 μm). **B**, 3D construction of FB-VEGF-C-treated wound images shows $CD45^+$ cells located in the lymphatic lumen. The arrows indicate leukocytes found at the apical site of lymphatic vessels, suggesting that those cells completed the transmigration process (scale bar, 20 μm). **C**, The total amount of $CD45^+$ cells per mm^2 of granulation tissue in the wound was calculated using fluorescent confocal images. **D**, Quantification of total $CD45^+$ cells detected in Lyve-1^+ lymphatic lumen per mm^2 wound tissue ($n \geq 5$,*$p < 0.05$). **E**, Confocal images of wound sections labeled with Lyve-1 (green) and CCL21 (red). The arrows show perinuclear CCL21 deposited in Lyve-1^+ vessels (Scale bar: 10 μm). **F**, Average intensity of CCL21 per μm^2 granulation wound tissue ($n \geq 4$, **$p < 0.01$).

delivery method for therapeutic efficacy of VEGF-C, similar to that shown for VEGF-A [39], and introduce both a means of inducing local lymphangiogenesis as well as a potential therapeutic application.

Contributions

E.G, M.A.S., W.W.K conceived the study and designed the experiments and wrote the manuscript; J.A.H. designed the

Fig. 7. Lymphangiogenic gels accelerate wound healing in diabetic mice. **A,** Full-thickness back skin wounds were created on db/db mice, and the wounds were treated with fibrin gels (control or with 200 ng VEGF-C or FB-VEGF-C) for 10 days. Wound sections were stained for H&E, and representative images show the GT thickness of each group. A black arrow shows the initial wound edges, while a red arrow shows the tip of re-epithelization (Scale bar: 500μm). (**B**) GT thickness and (**C**) percent wound re-epithelization were analyzed using H&E-stained tissue sections. **D,** Lymphatic vessel density was assessed by immunofluorescence staining (DAPI: blue, Lyve-1: green, podoplanin: red, magnification 40×, scale bar: 80 μm) and quantified by measuring (**E**) the percent area of Lyve-1^+ pixel area per mm^2 of granulation tissue. **F,** The percentage of vessels larger than 1200 μm^2 in GT. Lyve-1^+ area per vessel was calculated per sample. Samples with a Lyve-1^+ area <40 μm^2 and samples that had less than 6 vessels were removed from the analysis. Lyve-1^+ pixels forming a lumen counted as a vessel, and the size distribution was normalized to the total number of vessels for each condition ($n \geq 7$, mean ± SD, *$p < 0.05$, **$p < 0.01$, ***$p < 0.001$).

experiments and provided expertise; E.G., P.S.B, W.W.K., D.F., M.A.F performed the experiments.

Competing financial interests

The authors declare no competing financial interests.

Acknowledgements

The authors are grateful to S. Hirosue for editing the manuscript and advice, C. Buchanan, V. Triacca, J.P. Gaudry, M. Pasquier, P.C. Henrioud, Y. Ben Saida and E. Buck for their technical assistance and advice. The authors are grateful to the EPFL Bioimaging and Optics Platform and Histology Core facility for their technical assistance. Funding for this project was provided in part from the European Commission Framework Project 7 Angioscaff, and from the European Research Commission Advanced Grant LymphImmune, 323053.

Appendix A. Supplementary data

Supplementary data related to this article can be found at http://dx.doi.org/10.1016/j.biomaterials.2017.03.033.

References

[1] L.A. Johnson, D.G. Jackson, Control of dendritic cell trafficking in lymphatics by chemokines, Angiogenesis 17 (2014) 335–345.
[2] C.M. Card, S.S. Yu, M.A. Swartz, Emerging roles of lymphatic endothelium in regulating adaptive immunity, J. Clin. Invest. 124 (2014) 943–952.
[3] E. Kukk, A. Lymboussaki, S. Taira, A. Kaipainen, M. Jeltsch, V. Joukov, et al., VEGF-C receptor binding and pattern of expression with VEGFR-3 suggests a role in lymphatic vascular development, Development 122 (1996) 3829–3837.
[4] M.G. Achen, M. Jeltsch, E. Kukk, T. Makinen, A. Vitali, A.F. Wilks, et al., Vascular endothelial growth factor D (VEGF-D) is a ligand for the tyrosine kinases VEGF receptor 2 (Flk1) and VEGF receptor 3 (Flt4), Proc. Natl. Acad. Sci. U. S. A. 95 (1998) 548–553.
[5] M.A. Swartz, M. Skobe, Lymphatic function, lymphangiogenesis, and cancer metastasis, Microsc. Res. Tech. 55 (2001) 92–99.
[6] J.J. Tomasek, G. Gabbiani, B. Hinz, C. Chaponnier, R.A. Brown, Myofibroblasts and mechano-regulation of connective tissue remodelling, Nat. Rev. Mol. Cell Biol. 3 (2002) 349–363.
[7] W.W. Kilarski, B. Samolov, L. Petersson, A. Kvanta, P. Gerwins, Biomechanical regulation of blood vessel growth during tissue vascularization, Nat. Med. 15 (2009) 657–664.
[8] W.W. Kilarski, P. Gerwins, A new mechanism of blood vessel growth - hope for new treatment strategies, Discov. Med. 15 (2009) 23–27.
[9] P. Baluk, A. Hogmalm, M. Bry, K. Alitalo, K. Bry, D.M. McDonald, Transgenic overexpression of interleukin-1beta induces persistent lymphangiogenesis but not angiogenesis in mouse airways, Am. J. Pathol. 182 (2013) 1434–1447.
[10] C. Norrmen, T. Tammela, T.V. Petrova, K. Alitalo, Biological basis of therapeutic lymphangiogenesis, Circulation 123 (2011) 1335–1351.
[11] K. Paavonen, P. Puolakkainen, L. Jussila, T. Jahkola, K. Alitalo, Vascular endothelial growth factor receptor-3 in lymphangiogenesis in wound healing, Am. J. Pathol. 156 (2000) 1499–1504.
[12] J. Goldman, J.M. Rutkowski, J.D. Shields, M.C. Pasquier, Y. Cui, H.G. Schmokel, et al., Cooperative and redundant roles of VEGFR-2 and VEGFR-3 signaling in adult lymphangiogenesis, FASEB J. 21 (2007) 1003–1012.
[13] J.M. Rutkowski, K.C. Boardman, M.A. Swartz, Characterization of lymphangiogenesis in a model of adult skin regeneration, Am. J. Physiol. Heart Circ. Physiol. 291 (2006) H1402–H1410.
[14] C.P. Ng, M.A. Swartz, Fibroblast alignment under interstitial fluid flow using a novel 3-D tissue culture model, Am. J. Physiol. Heart Circ. Physiol. 284 (2003) H1771–H1777.
[15] W.W. Kilarski, L. Petersson, P.F. Fuchs, M.S. Zielinski, P. Gerwins, An in vivo neovascularization assay for screening regulators of angiogenesis and assessing their effects on pre-existing vessels, Angiogenesis 15 (2012) 643–655.
[16] D.A. Rigby, D.J. Ferguson, L.A. Johnson, D.G. Jackson, Neutrophils rapidly transit inflamed lymphatic vessel endothelium via integrin-dependent proteolysis and lipoxin-induced junctional retraction, J. Leukoc. Biol. 98 (2015) 897–912.
[17] W. Lawrance, S. Banerji, A.J. Day, S. Bhattacharjee, D.G. Jackson, Binding of hyaluronan to the native lymphatic vessel endothelial receptor LYVE-1 is critically dependent on receptor clustering and hyaluronan organization, J. Biol. Chem. 291 (2016) 8014–8030.
[18] K. Maruyama, J. Asai, M. Ii, T. Thorne, D.W. Losordo, P.A. D'Amore, Decreased macrophage number and activation lead to reduced lymphatic vessel formation and contribute to impaired diabetic wound healing, Am. J. Pathol. 170 (2007) 1178–1191.
[19] T. Tammela, A. Saaristo, T. Holopainen, J. Lyytikka, A. Kotronen, M. Pitkonen, et al., Therapeutic differentiation and maturation of lymphatic vessels after lymph node dissection and transplantation, Nat. Med. 13 (2007) 1458–1466.
[20] A. Saaristo, T. Tammela, A. Farkkilä, M. Kärkkäinen, E. Suominen, S. Yla-Herttuala, et al., Vascular endothelial growth factor-C accelerates diabetic wound healing, Am. J. Pathol. 169 (2006) 1080–1087.
[21] A. Szuba, M. Skobe, M.J. Karkkainen, W.S. Shin, D.P. Beynet, N.B. Rockson, et al., Therapeutic lymphangiogenesis with human recombinant VEGF-C, FASEB J. 16 (2002) 1985–1987.
[22] S.E. Epstein, R. Kornowski, S. Fuchs, H.F. Dvorak, Angiogenesis therapy: amidst the hype, the neglected potential for serious side effects, Circulation 104 (2001) 115–119.
[23] K. Lee, E.A. Silva, D.J. Mooney, Growth factor delivery-based tissue engineering: general approaches and a review of recent developments, J. R. Soc. Interface 8 (2011) 153–170.
[24] A. Saaristo, T. Veikkola, B. Enholm, M. Hytonen, J. Arola, K. Pajusola, et al., Adenoviral VEGF-C overexpression induces blood vessel enlargement, tortuosity, and leakiness but no sprouting angiogenesis in the skin or mucous membranes, FASEB J. 16 (2002) 1041–1049.
[25] V. Joukov, T. Sorsa, V. Kumar, M. Jeltsch, L. Claesson-Welsh, Y. Cao, et al., Proteolytic processing regulates receptor specificity and activity of VEGF-C, EMBO J. 16 (1997) 3898–3911.
[26] N. Isaka, T.P. Padera, J. Hagendoorn, D. Fukumura, R.K. Jain, Peritumor lymphatics induced by vascular endothelial growth factor-C exhibit abnormal function, Cancer Res. 64 (2004) 4400–4404.
[27] A.C. Mitchell, P.S. Briquez, J.A. Hubbell, J.R. Cochran, Engineering growth factors for regenerative medicine applications, Acta Biomater. 30 (2016) 1–12.
[28] P.S. Briquez, J.A. Hubbell, M.M. Martino, Extracellular matrix-inspired growth factor delivery systems for skin wound healing, Adv. Wound Care (New Rochelle) 4 (2015) 479–489.
[29] M. Ehrbar, V.G. Djonov, C. Schnell, S.A. Tschanz, G. Martiny-Baron, U. Schenk, et al., Cell-demanded liberation of VEGF-121 from fibrin implants induces local and controlled blood vessel growth, Circ. Res. 94 (2004) 1124–1132.
[30] P.A. Janmey, J.P. Winer, J.W. Weisel, Fibrin gels and their clinical and bioengineering applications, J. R. Soc. Interface 6 (2009) 1–10.
[31] S. Podgrabinska, P. Braun, P. Velasco, B. Kloos, M.S. Pepper, M. Skobe, Molecular characterization of lymphatic endothelial cells, Proc. Natl. Acad. Sci. U. S. A. 99 (2002) 16069–16074.
[32] J.C. Schense, J.A. Hubbell, Cross-linking exogenous bifunctional peptides into fibrin gels with factor XIIIa, Bioconj. Chem. 10 (1999) 75–81.
[33] M.P. Lutolf, J.L. Lauer-Fields, H.G. Schmoekel, A.T. Metters, F.E. Weber, G.B. Fields, et al., Synthetic matrix metalloproteinase-sensitive hydrogels for the conduction of tissue regeneration: engineering cell-invasion characteristics, Proc. Natl. Acad. Sci. U. S. A. 100 (2003) 5413–5418.
[34] C.P. Ng, B. Hinz, M.A. Swartz, Interstitial fluid flow induces myofibroblast differentiation and collagen alignment in vitro, J. Cell Sci. 118 (2005) 4731–4739.
[35] M.M. Martino, F. Tortelli, M. Mochizuki, S. Traub, D. Ben-David, G.A. Kuhn, et al., Engineering the growth factor microenvironment with fibronectin domains to promote wound and bone tissue healing, Sci. Transl. Med. 3 (2011), 100ra89.
[36] M.M. Martino, P.S. Briquez, A. Ranga, M.P. Lutolf, J.A. Hubbell, Heparin-binding domain of fibrin(ogen) binds growth factors and promotes tissue repair when incorporated within a synthetic matrix, Proc. Natl. Acad. Sci. U. S. A. 110 (2013) 4563–4568.
[37] K.M. Lorentz, S. Kontos, P. Frey, J.A. Hubbell, Engineered aprotinin for improved stability of fibrin biomaterials, Biomaterials 32 (2011) 430–438.
[38] W.W. Kilarski, E. Güç, J.C.M. Teo, S.R. Oliver, A.W. Lund, M.A. Swartz, Intravital immunofluorescence for visualizing the microcirculatory and immune microenvironments in the mouse ear dermis, PLoS One 8 (2013) e57135.
[39] M.M. Martino, P.S. Briquez, E. Guc, F. Tortelli, W.W. Kilarski, S. Metzger, et al., Growth factors engineered for super-affinity to the extracellular matrix enhance tissue healing, Science 343 (2014) 885–888.
[40] M.A. Broggi, M. Schmaler, N. Lagarde, S.W. Rossi, Isolation of murine lymph node stromal cells, J. Vis. Exp. (2014) e51803.
[41] D. Seliktar, A.H. Zisch, M.P. Lutolf, J.L. Wrana, J.A. Hubbell, MMP-2 sensitive, VEGF-bearing bioactive hydrogels for promotion of vascular healing, J. Biomed. Mater Res. A 68 (2004) 704–716.
[42] C.L. Helm, M.E. Fleury, A.H. Zisch, F. Boschetti, M.A. Swartz, Synergy between interstitial flow and VEGF directs capillary morphogenesis in vitro through a gradient amplification mechanism, Proc. Natl. Acad. Sci. U. S. A. 102 (2005) 15779–15784.
[43] C.P. Ng, C.-L.E. Helm, M.A. Swartz, Interstitial flow differentially stimulates blood and lymphatic endothelial cell morphogenesis in vitro, Microvasc. Res. 68 (2004) 258–264.
[44] P. Baluk, S. Morikawa, A. Haskell, M. Mancuso, D.M. McDonald, Abnormalities of basement membrane on blood vessels and endothelial sprouts in tumors, Am. J. Pathol. 163 (2003) 1801–1815.
[45] D. Shepro, Microvascular Research: Biology and Pathology, Elsevier Academic Press, Amsterdam; Boston, 2006.
[46] V. Djonov, A.N. Makanya, New insights into intussusceptive angiogenesis, EXS

(2005) 17–33.
[47] W.W. Kilarski, A. Muchowicz, M. Wachowska, R. Mezyk-Kopec, J. Golab, M.A. Swartz, et al., Optimization and regeneration kinetics of lymphatic-specific photodynamic therapy in the mouse dermis, Angiogenesis 17 (2014) 347–357.
[48] E. Guc, M. Fankhauser, A. Lund, M.A. Swartz, W.W. Kilarski, Long-term intravital immunofluorescence imaging of tissue matrix components with epifluorescence and two-photon microscopy, J. Vis. Exp. 86 (2014) e51388.
[49] D. Roth, M. Piekarek, M. Paulsson, H. Christ, W. Bloch, T. Krieg, et al., Plasmin modulates vascular endothelial growth factor-A-mediated angiogenesis during wound repair, Am. J. Pathol. 168 (2006) 670–684.
[50] I.G. Kim, J.Y. Lee, D.S. Lee, J.Y. Kwon, J.H. Hwang, Extracorporeal shock wave therapy combined with vascular endothelial growth factor-C hydrogel for lymphangiogenesis, J. Vasc. Res. 50 (2013) 124–133.
[51] R. Forster, A.C. Davalos-Misslitz, A. Rot, CCR7 and its ligands: balancing immunity and tolerance, Nat. Rev. Immunol. 8 (2008) 362–371.
[52] C. Beauvillain, P. Cunin, A. Doni, M. Scotet, S. Jaillon, M.L. Loiry, et al., CCR7 is involved in the migration of neutrophils to lymph nodes, Blood 117 (2011) 1196–1204.
[53] A. Issa, T.X. Le, A.N. Shoushtari, J.D. Shields, M.A. Swartz, Vascular endothelial growth factor-C and C-C chemokine receptor 7 in tumor cell-lymphatic cross-talk promote invasive phenotype, Cancer Res. 69 (2009) 349–357.
[54] K.M. Lorentz, L. Yang, P. Frey, J.A. Hubbell, Engineered insulin-like growth factor-1 for improved smooth muscle regeneration, Biomaterials 33 (2012) 494–503.
[55] J. Goldman, T.X. Le, M. Skobe, M.A. Swartz, Overexpression of VEGF-C causes transient lymphatic hyperplasia but not increased lymphangiogenesis in regenerating skin, Circ. Res. 96 (2005) 1193–1199.
[56] M. Jeltsch, A. Kaipainen, V. Joukov, X. Meng, M. Lakso, H. Rauvala, et al., Hyperplasia of lymphatic vessels in VEGF-C transgenic mice, Science 276 (1997) 1423–1425.
[57] W.L. Olszewski, P. Jain, M. Zaleska, E. Stelmach, E. Swoboda, Chronic lower limb wounds evoke systemic response of the lymphatic (immune) system, Indian J. Plast. Surg. 45 (2012) 255–260.
[58] A.M. Venugopal, R.H. Stewart, G.A. Laine, C.M. Quick, Nonlinear lymphangion pressure-volume relationship minimizes edema, Am. J. Physiol. Heart Circ. Physiol. 299 (2010) H876–H882.
[59] M.A. Swartz, A. Kaipainen, P.A. Netti, C. Brekken, Y. Boucher, A.J. Grodzinsky, et al., Mechanics of interstitial-lymphatic fluid transport: theoretical foundation and experimental validation, J. Biomech. 32 (1999) 1297–1307.
[60] K.C. Boardman, M.A. Swartz, Interstitial flow as a guide for lymphangiogenesis, Circ. Res. 92 (2003) 801–808.
[61] P. Baluk, J. Fuxe, H. Hashizume, T. Romano, E. Lashnits, S. Butz, et al., Functionally specialized junctions between endothelial cells of lymphatic vessels, J. Exp. Med. 204 (2007) 2349–2362.
[62] T. Lammermann, B.L. Bader, S.J. Monkley, T. Worbs, R. Wedlich-Soldner, K. Hirsch, et al., Rapid leukocyte migration by integrin-independent flowing and squeezing, Nature 453 (2008) 51–55.
[63] L.-C. Yao, P. Baluk, R.S. Srinivasan, G. Oliver, D.M. McDonald, Plasticity of button-like junctions in the endothelium of airway lymphatics in development and inflammation, Am. J. Pathol. 180 (2012) 2561–2575.
[64] M.S. Pepper, M. Skobe, Lymphatic endothelium: morphological, molecular and functional properties, J. Cell Biol. 163 (2003) 209–213.
[65] A. Saaristo, T. Tammela, J. Timonen, S. Yla-Herttuala, E. Tukiainen, S. Asko-Seljavaara, et al., Vascular endothelial growth factor-C gene therapy restores lymphatic flow across incision wounds, FASEB J. 18 (2004) 1707–1709.
[66] C. Wetzler, H. Kampfer, B. Stallmeyer, J. Pfeilschifter, S. Frank, Large and sustained induction of chemokines during impaired wound healing in the genetically diabetic mouse: prolonged persistence of neutrophils and macrophages during the late phase of repair, J. Invest. Dermatol. 115 (2000) 245–253.
[67] H. Saeki, A.M. Moore, M.J. Brown, S.T. Hwang, Cutting edge: secondary lymphoid-tissue chemokine (SLC) and CC chemokine receptor 7 (CCR7) participate in the emigration pathway of mature dendritic cells from the skin to regional lymph nodes, J. Immunol. 162 (1999) 2472–2475.
[68] L.A. Johnson, S. Clasper, A.P. Holt, P.F. Lalor, D. Baban, D.G. Jackson, An inflammation-induced mechanism for leukocyte transmigration across lymphatic vessel endothelium, J. Exp. Med. 203 (2006) 2763–2777.
[69] T. Hoshida, N. Isaka, J. Hagendoorn, E. di Tomaso, Y.-L. Chen, B. Pytowski, et al., Imaging steps of lymphatic metastasis reveals that vascular endothelial growth factor-C increases metastasis by increasing delivery of cancer cells to lymph nodes: therapeutic implications, Cancer Res. 66 (2006) 8065–8075.
[70] D.M. Fonseca, T.W. Hand, S.J. Han, M.Y. Gerner, A. Glatman Zaretsky, A.L. Byrd, et al., Microbiota-dependent sequelae of acute infection compromise tissue-specific immunity, Cell 163 (2015) 354–366.
[71] P. Baluk, T. Tammela, E. Ator, N. Lyubynska, M.G. Achen, D.J. Hicklin, et al., Pathogenesis of persistent lymphatic vessel hyperplasia in chronic airway inflammation, J. Clin. Invest. 115 (2005) 247–257.
[72] T.V. Petrova, T. Karpanen, C. Norrmen, R. Mellor, T. Tamakoshi, D. Finegold, et al., Defective valves and abnormal mural cell recruitment underlie lymphatic vascular failure in lymphedema distichiasis, Nat. Med. 10 (2004) 974–981.